NUMERICAL STUDY OF EROSION WEAR ON A CENTRIFUGAL SLURRY PUMP

Thesis submitted in partial fulfilment of the requirements for the award of degree of

Master of Engineering

in

CAD/CAM & ROBOTICS

Thapar University, Patiala

By:

Abhineet Kumar Sharma

Roll No. 80681001

Under the supervision of:

Mr. Satish Kumar

Lecturer, MED

JUNE 2008

MECHANICAL ENGINEERING DEPARTMENT

THAPAR UNIVERSITY

PATIALA – 147004

CERTIFICATE

I hereby certify that the work which is being presented in the thesis entitled, "**NUMERICAL STUDY OF EROSION WEAR ON A CENTRIFUGAL SLURRY PUMP** ", in partial fulfilment of the requirements for the award of degree of Master of Engineering in Mechanical Engineering with specialization in **CAD/CAM & ROBOTICS** submitted in **Mechanical Engineering Department** of Thapar University, Patiala, is an authentic record of my own work carried out under the supervision of **Mr. Satish Kumar** and refers other researcher's works which are duly listed in the reference section.

The matter presented in this thesis has not been submitted for the award of any other degree of this or any other university.

Abhineet Kumar Sharma

This is to certify that the above statement made by the candidate is correct and true to the best of my knowledge.

Satish Kumar
Lecturer, MED
Thapar University
Patiala

Dr .S.K MOHAPATRA
Professor & Head
Mechanical Engineering Department
Thapar University,
Patiala

R.K.SHARMA
Dean (Academic Affairs)
Thapar University,
Patiala.

ACKNOWLEDGMENT

Working without proper guidance and expecting success is just like making castles in the air, so whenever one wants to start any work, he requires guidance from experts. I express my sincere gratitude to my guide ,Mr. Satish Kumar, lecturer , Department of Mechanical Engineering, Thapar University**,** for acting as supervisor and giving valuable guidance during the course of this investigation, for his ever encouraging and timely moral support. His enormous knowledge and intelligence always helped me unconditionally to solve various problems.

I am greatly thankful to Dr. S. K. Mohapatra, Professor and Head, Mechanical Engineering Department, Thapar University for his encouragement and inspiration for execution of the thesis work. I do not find enough words with which I can express my feeling of thanks to entire faculty and staff of Department of Mechanical Engineering, Thapar University, Patiala for their help, inspiration and moral support, which went a long way in successfully completion of my thesis.

Abhineet Kumar Sharma

ABSTRACT

Slurry erosion is a crucial problem in many industrial applications, due to impingement of solid particles being suspended in the fluids flowing at high velocity. It affects both the initial cost and life of the component. Erosive wear can be found on impellers & volute casing in slurry pumps, angled pipe bends, turbines, pipes and pipe fitting, nozzles, burners etc. The volume loss due to erosion is a troublesome problem for slurry transportation. The service life of equipments handling solid–liquid mixture can be increased by reducing the erosion wear. It is therefore necessary to study erosion wear systematically, so that efforts can be made to minimize the wear during design stage. Centrifugal pumps are generally used for slurry transport. Due to erosion, the life of pumps used is very short and they need to replace periodically.

In the present work a systematic study on the erosion wear has been carried out to improve the present understanding .Numerical simulation has been carried out for radial flow impeller and the effect of affecting parameters on erosion wear has been studied .The results clearly indicated that all factors contribute to wear of centrifugal pump impeller. The erosion rate of blades is 10 times greater than the erosion wear of hub. The erosion rate is found to be more severe near the leading edge as compared to other parts of impeller. The simulations which were carried out on impeller show that particle size affects the erosion rate only up to certain size of particles and depends on the impact angle.

CONTENTS

LIST OF FIGURES

LIST OF TABLES

NOMENCLATURE

SYMBOLS	STANDS FOR
N	Speed at which pump shaft rotates
Q	Discharge in m^3 / sec
H	Net head in m.
N_s	Specific Speed
P_o	Output power
$P_{in,}$	Input power
P_{sh}	Shaft Power
ρ	Density of the fluid
g	Acceleration due to gravity
η_h	Hydraulic Efficiency
η_o	Overall Efficiency
η_m	Mechanical Efficiency
T	Torque transmitted by the shaft
F_s	Allowable shear stress
D_{sh}	Shaft diameter
D_{hb}	Hub diameter
C_A	Axial Velocity at entry of impeller.
C_1	Absolute Velocity at inlet of the blade
C_3	Absolute Velocity at eye of the blade.
D_1	Diameter at the inlet of the blade.
b_1	Breadth of the blade at the inlet
u_2	Blade velocity at outlet
u_1	Blade velocity at inlet
β_1	Blade inlet angle

H_r	Total head generated
Z	Number of blades
C_{2m}	Meridional flow velocity inside impeller
C_{1m}	Meridional Flow Velocity at suction end
B_2	Width of blade at Outlet
r_2	Outer radius of the blade
ω	Angular velocity of impeller
F_s	Shear stress
ε	Turbulence eddy dissipation (the rate at which the velocity fluctuations dissipate)
k	Turbulence kinetic energy per unit mass
B	Sum of body forces
μ_{eff}	Effective viscosity accounting for turbulence
μ_t	Turbulence viscosity
w	Turbulence frequency
F_2	Blending function
S	Strain rate.
α	Continuous phase
β	Dispersed phase
$A_{\alpha\beta}$	Surface area per unit volume
d_β	Mean diameter of spherical particles
r_β	Minimum volume fraction
V_p	Particle impact velocity
v_{pi}	Particle velocity
t	Time in seconds
E	Dimensionless mass (Mass of eroded wall material divided by the mass of particle)

V_p	Particle impact velocity
γ	Impact angle in radians between the approaching particle track and the wall
γ_0	Angle of maximum erosion
$f(\gamma)$	Dimensionless function of the impact angle
u	Component of velocity in x-direction
v	Component of velocity in y-direction
B_1	Width of blade at outlet
ΔH	Net Positive Suction Head (NPSH)
p	Pfleiderer's coefficient
μ_t	Turbulent viscosity

CHAPTER 1

INTRODUCTION

1.1 SLURRY

Slurry is a mixture of solids and liquids. Its physical characteristics are dependent on many factors such as size and distribution of particles, concentration of solids in the liquid phase, size of the conduit, level of turbulence, temperature, and absolute (or dynamic) viscosity of the carrier. Nature offers examples of slurry flows such as seasonal floods that carry silt and gravel. A slurry mixture is a mixture of a carrying fluid and solid particles held in suspension. The most commonly used fluid is water, however in some cases air is also used such as in pneumatic conveying. Theoretically, a single-phase liquid of low absolute (or dynamic) viscosity can be allowed to flow at slow speeds from a laminar flow to a turbulent flow. However, a two-phase mixture, such as slurry, must overcome a deposition critical velocity or a viscous transition critical velocity. If the slurry's speed of flow is not sufficiently high, the particles will not be maintained in suspension. On the other hand, in the case of highly viscous mixtures, if the shear rate in the pipeline is excessively low, the mixture will be too viscous and will resist flow.

1.2 TYPES OF SLURRY FLOWS

There are generally two types of flows:

1.2.1 Homogeneous flows

In homogeneous flows solids are uniformly distributed throughout the liquid carrier. For example copper concentrate slurry after undergoing a process of grinding and thickening. Drilling mud, sewage sludge, and fine limestone behave as homogeneous flows.

1.2.2 Heterogeneous flows

In heterogeneous flows, solids are not uniformly mixed in the horizontal plane. Heavier particles tend to settle down and lighter particles tend to float. Sliding bed

may form in the pipe, with the heavier particles at the bottom and the lighter ones in suspension. Heterogeneous slurries are encountered in many places mining, phosphate rock mining, and dredging applications. Heterogeneous flows require a minimum carrier velocity.

Although the transportation of solids in the form of slurries is basically older than history.The blood circulating system in mammals involves the use of a positive displacement pump forcing slurry of solid corpuscles in liquid serum through a complex pipeline. The slurry transportation of solids through long pipelines and with the help of centrifugal pumps has been undertaken only in almost last 25 years.

1.3 PUMPS

A pump is a device used to move liquids or slurries. A pump moves liquids from lower pressure to higher pressure. Machine that draws a fluid into itself through an

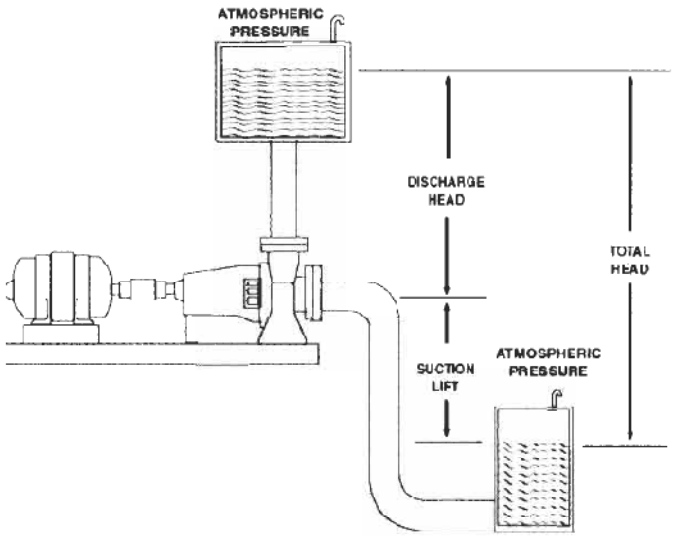

Figure 1.1 A schematic diagram showing pump installation

entrance port and forces the fluid out through an exhaust port. A pump may serve to move liquid, as in a cross-country pipeline; to lift liquid, as from a well or to the top of a tall building; or to put fluid under pressure, as in a hydraulic brake. These applications depend predominantly upon the discharge characteristics of the pump. Figure 1.1 shows the schematic diagram of the pump.

1.3.1 Types of Pumps

The three basic types of pumps are centrifugal, reciprocating, and rotary.

1.3.1.1 Reciprocating pump

In reciprocating pumps the mechanical energy is converted into hydraulic energy by sucking the liquid into a cylinder in which a piston is reciprocating (moving backwards and forwards) which exerts the thrust on the liquid and increases its hydraulic energy(pressure energy), the pump is known as reciprocating pump. Reciprocating pumps are used where a precise amount of liquid is required to be delivered, also where the delivery pressure required is higher than that can be achieved with other types. Figure 1.2 shows line diagram of reciprocating pump.

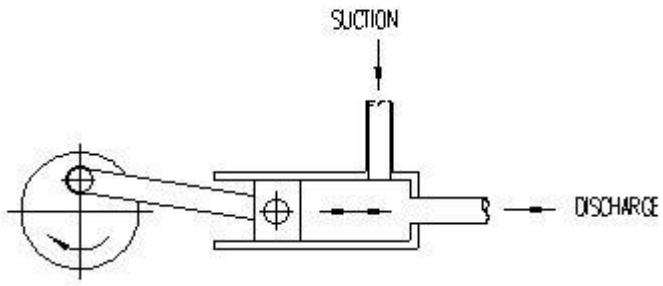

Figure 1.2 Reciprocating pump

1.3.1.2 Rotary pump

Rotary pump is used to move heavy or very viscous fluids.These employ mechanical means such as gear, cam and screw to move the liquid

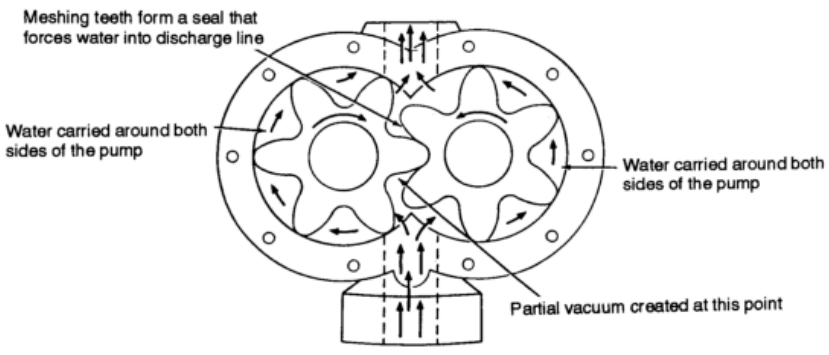

Figure 1.3: Sectional view of rotary pump

Figure 1.4: Model of a centrifugal pump

1.4 CENTRIFUGAL PUMPS

The hydraulic machines, which convert the mechanical energy into hydraulic energy, are called pumps. The hydraulic energy is in the form of pressure energy. The mechanical energy is converted into pressure energy by means of centrifugal force acting on the fluid; the hydraulic machines are called centrifugal pumps. The flow in a centrifugal pump is in radial outward direction. Figure 1.4 shows the 3 dimensional model of a centrifugal pump.

1.4.1 Working principle of centrifugal pump

The centrifugal pump works on the principle of forced vortex flow, which means that when a certain mass of liquid is rotated by an external flow, the rise in pressure head of the rotating liquid takes place. The rise in pressure head at any point of the rotating liquid is proportional to the square of tangential velocity of the liquid at that point. Thus at the outlet of the impeller where the radius is more, the rise in pressure head will be more and the liquid will be discharged at the outlet with high pressure head. Due to high-pressure head, the liquid can be lifted to a high level. Figure 1.5 shows flow of fluid in a centrifugal pump.

1.4.2 Advantages of using centrifugal pumps for transportation of slurry

1) Simplicity of design

2) Easier installation

3) Low maintenance

4) Lower weight

5) Handles suspensions and slurry easily

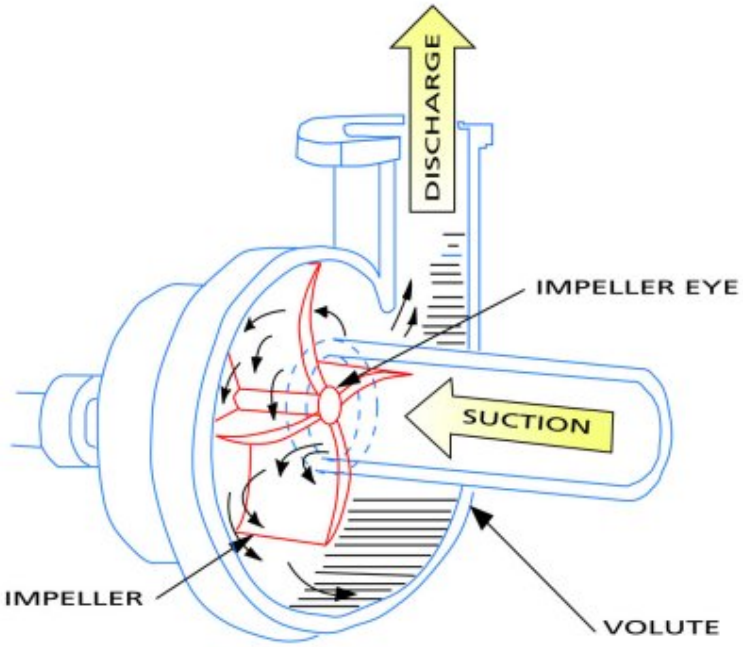

Figure 1.5 Flow of fluid in a centrifugal pump

1.4.3 Types of centrifugal pumps

Centrifugal pumps can be classified into three general categorized according to the way the impeller imparts energy to the fluid. Each of these categories has a range of specific speeds and appropriate applications.

The three main categories of centrifugal pumps:

1) Radial flow Impeller

2) Mixed Flow Impeller

3) Axial flow Impeller

1.4.3.1. Radial flow impeller

Most centrifugal pumps are of radial flow. Radial flow impellers impart energy primarily by centrifugal force. Water enters the hub and flows radically to the periphery. Flow leaves the impeller at 90 degree angle from the direction it enters the pump.

1.4.3.2. Mixed flow impeller

Mixed flow impellers impart energy partially by centrifugal force and partially as an axial compressor. This type of pump has a single inlet impeller with flow entering axially and discharging in an axial and radial direction. Mixed flow impellers are suitable for pumping untreated waste water. They operate at high speeds than the radial flow impeller pumps; are usually of lighter construction; and where applicable, cost less than other pumps. Impeller may be either open or enclosed, but enclosed is preferred.

1.4.3.3. Axial flow impeller

Axial flow impeller imparts energy to the water by acting as axial flow compressors. The axial flow pump has a single inlet impeller with flow entering and exiting along the axis of rotation (along the pump drive shaft). These pumps are used in low head, large capacity applications such as water supplies, irrigation, drainage etc.

1.4.4 Main parts of a centrifugal pump

The following are the main parts of centrifugal pumps

1) Impeller

2) Casing

3) Suction pipes with a foot valve and a strainer

4) Delivery pipe

1.4.4.1 Impeller

The rotating part of centrifugal pump is called impeller. It consists of a series of backward curved vanes. The impeller is mounted on a shaft, which is connected to the shaft of an electric motor. An impeller is usually made of iron, steel, aluminium or plastic, which transfers energy from the motor that drives the pump to the fluid being

pumped by forcing the fluid outwards from the centre of rotation. Figure 1.6a shows the axial, radial and tangential component of flow.

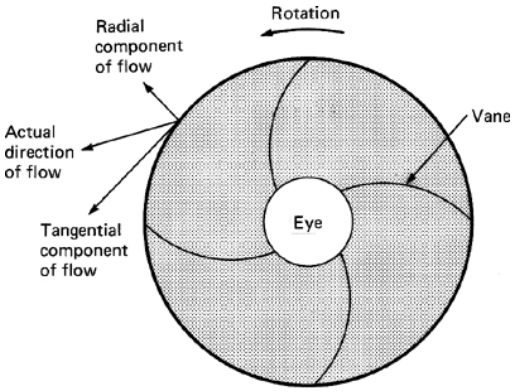

Figure 1.6a Front view of impeller **Figure 1.6b 3D model of impeller**

Components of impeller

a) Blade

Blades are the series of backward or forward curved vanes which transfers the power from shaft to the fluid.

b) Hub and Shroud

The hub is the surface of the machine closest to the axis of rotation. It defines the inner fluid flow surface. The shroud is the surface of the machine farthest from the axis of rotation. It defines the outer fluid flow surface. The hub and shroud can be defined only after the machine data has been defined, although all of these objects can be defined in one step.

c) Leading and trailing edges

The leading edge curve is the most upstream part of the blade. Any change to the leading edge changes the blade surfaces, which changes the periodic surfaces as well as the hub and shroud surfaces. The trailing edge curve is the most downstream part of the blade.

Impellers are also classified as to whether they are:

a) Open impellers:

Most totally open impellers are found on axial flow pumps. This type of impeller would be used in a somewhat conventional appearing pump to perform a chopping,

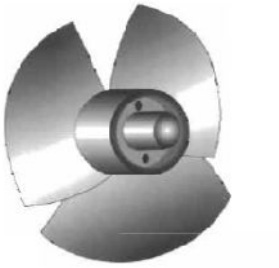

Figure 1.7 Open Impeller

grinding action on the liquid. The totally open axial flow impeller moves a lot of volume flow, but not a lot of head or pressure. With its open tolerances for moving and grinding solids, they are generally not high efficiency devices.

b) Semi-open impeller

Figure 1.8 Semi-Open Impeller

A semi-open impeller has exposed blades, but with a support plate or shroud on one side. These types of impeller are generally used for liquids with a small percentage of solid particles from the bottom of a tank or river, or crystals mixed with the liquid. The efficiency of these impellers is governed by the limited free space or tolerance between the front leading edge of the blades and the internal pump housing wall.

c) Enclosed impeller

Totally enclosed impellers are designed with the blades between two support shrouds or plates. These impellers are generally used clean liquids because tolerances are tight at the eye and the housing,and there is no room for suspended solids, crystals or sediment, Figure 1.9. shows a type of enclosed impeller

Figure 1.9 Enclosed Impeller

Cavitation damage, play in the bearings, bent shafts and unbalanced rotary assemblies, and any hydraulic side loading on the shaft and impeller assembly.

1.4.4.2 Casing

Casing of a pump is an airtight passage surrounding the impeller and is designed in such a way that the kinetic energy of the water discharged at outlet of the impeller is converted into the pressure energy before the water leaves the casing and enters the delivery pipe.

Types of casing:

a) Volute casing

Volute casing is of spiral type in which area of flow increase gradually. The increase in the area of flow decreases the velocity of flow.The decrease in velocity increases the pressure of the water flowing through the casing. In case of volute casing the efficiency of the pump increase slightly as a large amount of energy is lost due to formation of eddies in this type of casing.

b) Vortex casing

If a circular chamber is introduced between the casing and the impeller, the casing is known as vortex casing. By introducing the circular chamber, the loss of energy due to formation of eddies is reduced considerably. Thus, the efficiency of the pump is more than the pump with volute casing.

c) Casing with guide blades

In this type of casing, the impeller is surrounded by series of guide blades mounted on a ring, which is known as diffuser. The guide vanes are designed in such a way that water from the impeller enters the guide vanes without stock. Also the area of guide vanes increase, thus reducing the velocity of flow through guide vanes and consequently increasing the pressure of pressure of water. The water from the guide vanes then passes through the surrounding casing, which is concentric with the impeller

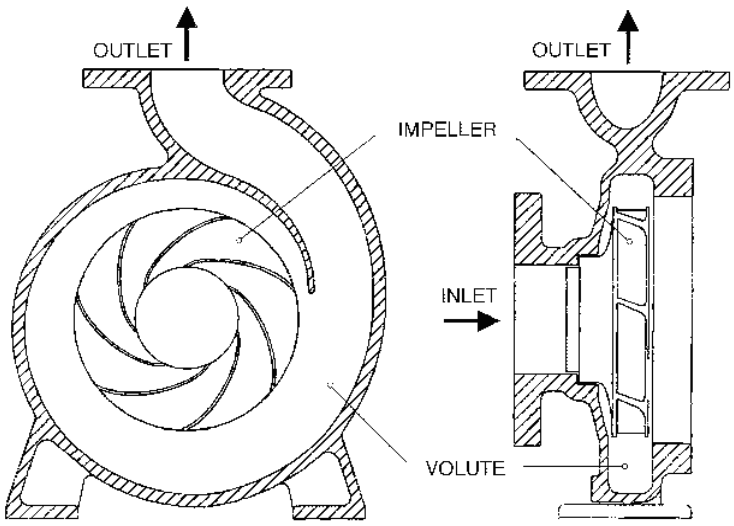

Figure 1.10 Sectional view of centrifugal pump

3) Suction pipe with a foot valve and a strainer

A pipe whose one end is connected to the inlet of the pump and the other end dips into water in a sump is known as a suction pipe. A foot valve, which is non-return valve or one-way type of valve, is fitted at the lower end of suction pipe. The foot valve opens only in the upward direction. A strainer is also fitted at the lower end of suction pipe

4) Delivery pipe

A pipe whose one end is connected to the outlet of the pump and the other delivers the water at the required height is known as delivery pipe.

1.4.5 Centrifugal pump applications

Pumps are used wherever any quantity of liquid must be moved from one place to another. Pumps are found in such services as steam power plants; water supply plants; sewage; drainage or irrigation; oil refineries, chemical plants and steel mills; food processing factories and mines; dredging or jetting operations; hydraulic power services and almost every ship whether driven by diesel or steam engine. While these pumps have much in common, they are varied to meet special requirements and particular needs of each service.

- Petroleum Industry
- Chemical Industry
- Textile Industries
- Paper Industry
- Sewage and Sump Services
- Irrigation, Drainage and Flood Control
- Mining and Construction

1.5 WEAR

Wear is defined as progressive volume loss of material from a solid surface due to corrosion, abrasion and erosion. Wear is one of the most common problems encountered in industrial applications. It is defined as the erosion of material from a solid surface by the action of another solid. In the domain of wear, particularly the wear encountered in handling abrasive solid particles, much work has been done in the past half century with regard to dry" abrasivity, but only in more recent years has interest grown in 'wet' abrasivity, namely slurries. Wear can be classified into following types

1.5.1 Types of wear

1.5.1.1 Adhesive wear

Adhesive wear is the only universal form of wear; it arises from the fact that, during sliding, regions of adhesive bonding, called junctions, form between the sliding surfaces. If one of these junctions does not break along its original interface, then a chunk from one of the sliding surfaces will have been transferred to the other surface. In this way, an adhesive wear particle will have been formed. Initially adhering to the other surface, adhesive particles soon become loose and can disappear from the sliding system.

One of the significant things about adhesive wear is that at the interface, or the point where it touches another metal surface, it must be very hot in order for the micro welding to take place at all. That is what adhesive wear is — microscopic welding. The heat produced at the contact interface is very high — near the melting point of the two metals touching each other. This heat mostly comes from the stress of contact and not from the temperature of the environment.

1.5.1.2 Abrasive wear

Abrasive wear is produced by a hard, sharp surface sliding against a softer one and digging out a groove. The abrasive agent may be one of the surfaces or it may be a third component (such as sand particles) Abrasive wear coefficients are large compared to adhesive ones. Thus, the introduction of abrasive particles into a sliding system can greatly increase the wear rate; automobiles, for example, have air and oil filters to catch abrasive particles before they can produce damage. On the abrasive specimen, the surface shows a scratched appearance from hard particles digging into it as they were moved across the surface.

1.5.1.3 Corrosive wear

Corrosive wear arises when a sliding surface is in a corrosive environment, and the sliding action continuously removes the protective corrosion layer, thus exposing fresh surface to further corrosive attack. Corrosive wear occurs as a result of chemical reaction on a wearing surface. The most common type of corrosion is mainly due to

reaction between metal and oxygen. These oxides are wiped away with the flow and cause pitting of the surfaces. Corrosion is accelerated as impacted surfaces are exposed to slurry chemistry.

1.5.1.4 Surface fatigue wear

Surface fatigue is a process by which the surface of a material is weakened by cyclic loading, which is one type of general material fatigue. Surface fatigue wear occurs as result of the formation and growth of cracks. It is the main form of wear of rolling devices such as ball bearings, wheels on rails, and gears. During continued rolling, a crack forms at or just below the surface and gradually grows until a large particle is lifted right out of the surface.

1.5.1.5 Erosive wear

Erosive wear is the dominant process and can be defined as the removal of material from a solid surface due to mechanical interaction between the surface and the impinging particles in a liquid stream. Erosion involves the transfer of kinetic energy to the surface. This means that in erosion material removal is a function of particle velocity squared to higher power. Erosive wear depends on the predominant impact angle of particle impingement with the material surface. Impact angle will vary from 0 to 90 degrees and depend on both fluid particle and particle- particle interaction. This type of wear can be found on impellers and volute casing in slurry pumps, angled pipe bends, turbines, pipes and pipe fitting, nozzles, burners etc. The material loss due to erosion increases with the increase in kinetic energy of the particles impacting at the target surface.

The volume loss due to erosion is a troublesome problem foe slurry transportation systems e.g. mineral transport systems, ash disposal systems. The erosion wear due to the air borne particles in some devices such as jet planes and turbines is also significant due to very high impact velocity. It is thus a challenging task to control the erosion wear in many engineering applications. The material removal due to erosion is caused by two dominant mechanisms namely brittle fractures and platelet deformations.

In brittle type material, the solid particles impacting on the target surface forms cracks in longitudinal and lateral directions. These cracks propagate due to impact of succeeding particles and broken materials pieces will be carried out by flowing fluid. The material removal rate due to brittle fracture increases with increase in normal component if the particle velocity and thus the brittle type material show maximum wear near normal impact angles.

In Platelet mechanism, the impact of solid particles deforms the target surface to forms hills and valleys. The repeated impacts of particles remove the material and forms crater at the surface. This mechanism along with micro-cutting and chipping dominates in ductile type materials, which show the maximum wear in the impact angle range of 20-40 degree. Apart from the target surface characteristics like brittle or ductile type, many other parameters such as solid particles, carrier fluid, flow conditions etc. affect the erosion wear. It is, therefore, difficult to estimate wear for a given operating conditions.

1.5.2 Parameters affecting erosion wear:

The prominent parameters and their effect on erosion wear are as under:

1) **Impact angle**

   Impact angle is defined as the angle between the target surface and the direction striking velocity of the solid particle. The variation of erosion wear with the impact angle depends on the characteristics of the target surface material namely brittle or ductile type.

2) **Velocity of solid particles**

   Velocity of solid particle strongly affects the erosion wear. As particle velocity increases there is significant increase in erosion rate. The erosion rate is generally related to the particle velocity using power law relationship in which the power index for velocity varies in the range of 2-4.

3) **Hardness**

   Hardness is the characteristic of a solid material expressing its resistance to permanent deformation.Surface hardness as well as hardness of solid particles has profound effect on the erosion wear mechanism. Hardness ratio has been defined as the ratio of hardness of target material to the hardness of solid particles.

4) **Particle size and shape**

Particle size and shape is also one of the prominent parameter, which affect erosion wear. Many investigators have considered solid particle size important to erosion. The erosion wear increases with increase in particle size according to power law relationship. The effect of particle shape on the erosion is not very well established due to difficulties in defining the different shape features. Generally roundness factor is taken into consideration. If roundness factor is one then the particles are perfectly spheres and a lower values show the particle angularity.

5) **Solid concentration**

Concentration is amount of solid particles by weight or by volume in the fluid. As concentration of particle increases more particles strike the surface of impeller which increase the erosion rate, the concentration of slurries can vary from 2% to 50% depending upon the type of slurry. However, at very high concentrations particle-particle interaction increases and this decreases the striking velocity of particle on the surface.

1.6 SLURRY EROSION TESTING

The erosion wear has been estimated by different ways such as field tests ,pilot plant tests, bench scale tests or numerical analysis. Field tests give the actual wear but required a long time and the results are particular to a specified condition. It is therefore preferable to conduct pilot plant test where the field conditions are to be simulated in a scaled test loop to generate data for different operating conditions with relatively less efforts. However, such tests are laborious, time consuming and require large materials.

Hence, most of the wear test data have been generated using bench scale test rigs. These rigs are suitable to small laboratory being small in size and some of the rigs can generate the data at an accelerated rate. The large data available for different Operating conditions have been generally used to develop empirical correlations for estimating erosion wear. In some of the numerical analysis, the correlations obtained through bench scale rigs have been used to estimate the erosion wear based on local values of the effecting parameters.

Erosion in slurry pumps can be tested by following methods:

1.6.1 Jet erosion test

In jet erosion, testing a high velocity jet strikes a flat specimen at some adjustable angle. In jet erosion tests, the amount of material removed is determined by the weight loss. The material which accumulates on the specimen surface interferes with the incoming particle. The weight loss of the specimen corresponds to the average erosion over the surface.

Jet erosion tester has been developed to investigate the effect of different parameters particularly the impact angle under controlled environment. In jet erosion tester, a circular jet of solid–liquid mixture strikes at the wear specimen fixed in a fixture, which can be oriented at any angle with respect to the former. Generally a pump is used to drive water at high pressure and the solid particles are being sucked through an injector. The mixing of the solid–liquid is formed in the mixing chamber before the jet comes out through a nozzle.

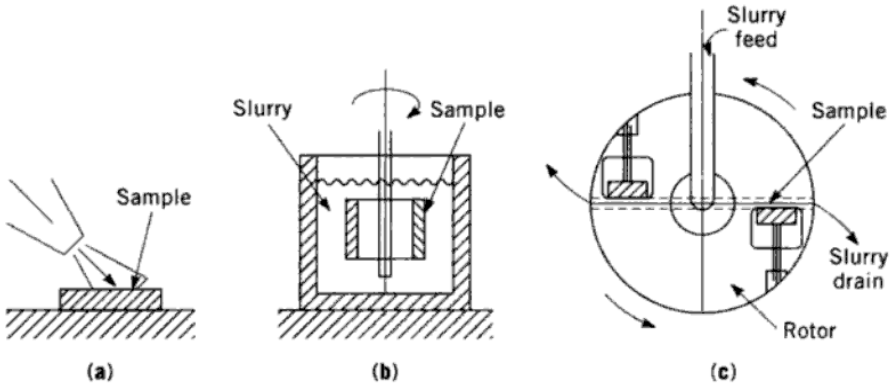

Figure 1.11 (a) Jet erosion tester (b) Slurry pot test (c) Coriolis erosion test

1.6.2 Slurry pot test

In slurry pots, a specimen rod of circular cross-section, fixed to the end of an arm, is rotated in a circular container filled with the slurry assuming homogeneous suspension of the solid particles. In slurry pot tests, also the amount of material removed is determined by the weight loss. The samples are weighted before and after the tests.

Slurry pot tester is simple in design, easy to fabricate and operate. In a slurry pot tester, generally two cylinder wear specimens have been rotated in solid –liquid mixture. The rotational movement of the wear specimens and sometimes an impeller attached at the end of 6^{th} shaft keep the solid particles suspended in the liquid. The rotating test specimen moves at a velocity relative to the solid-liquid suspension, which is assumed stationary and homogeneous inside the pot.

In a slurry pot tester the rotational velocity of the specimen has been taken as the relative velocity between the particles and wear specimens assuming suspension as stationary. However, due to rotation of the wear specimen and propeller the mixture inside the pot are highly turbulent conditions. Baffles are used to break the vortex produced, which also develops some amount of non-homogeneity in the suspension. These phenomena result in some error in evaluating the independent/isolated effect of various parameters such as velocity, concentration, and impact angle etc on erosion wear.

1.6.3 Coriolis erosion test

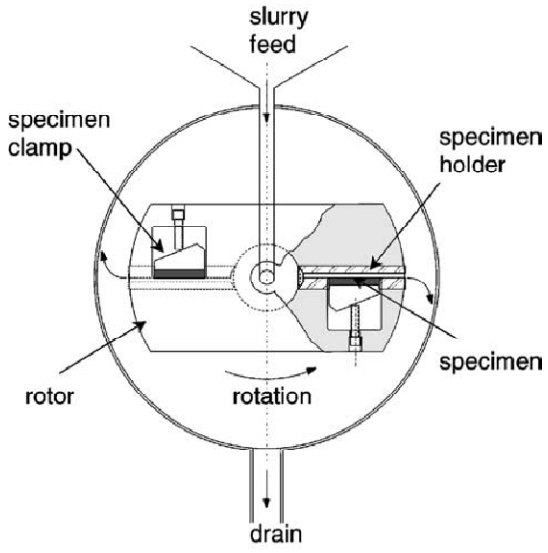

Figure 1.12 Schematic diagram of Coriolis erosion test

The Coriolis tester is used to simulate the motion of dense slurries and their interaction with surfaces such as slurry pumps or pipelines. In this type of tester slurry passes rapidly through a revolving rotor containing a wear specimen. In the Coriolis testing slurry is introduced into the centre of gravity of a rotor and exists through two radial channels. The specimen is mounted into the walls of a radial channel facing the

direction of rotation and is eroded by slurry particles, which are pressed against the specimen face by the Coriolis acceleration. The erosion groove is transversed using a profilometer and the local erosion depth is determined to with in a few microns. In the Coriolis erosion tester, a relatively small batch of slurry, from an over-head tank passes through the rotor in one pass. At rotor speeds of 6000 rpm, a measurable groove is worn into the specimen within a few minutes. Figure 1.12 shoes the schematic diagram of Coriolis erosion testing

1.6.4 Rotating pipe test

It consists of a circular pipe with wear pieces fitted at its inside surfaces and is filled with slurry with half of its capacity. The pipe ring was rotated at its own centre and relative motion between slurry and wear specimen causes erosion wear. This method is used to simulate pipeline erosion, but takes long time to generate wear data.

1.6.5 Concentric cylinder viscometer

In this type of test one cylinder was rotated inside a cylinder containing slurry. The wear at the outer wall of the inner cylinder surface was assumed to be cause by parallel flow of slurry.

CHAPTER 2

LITERATURE REVIEW

Desai P.V[1] [1990] has observed that erosion wear of centrifugal slurry pumps is primarily governed by the particulate motion and concentration as well as their physical properties. The analysis and the finite element computations yield the solid velocity and concentration fields in an arbitrary radial cross-section of a centrifugal slurry pump casing. The solutions were examined in light of their applicability to the pump wear problem. Axisymmetric finite elements have to be used to analyze the flow in the volume of revolution. The shape factor of the particles is introduced into the drag and pressure force calculations to account for the angularity of the particles.

Achim Daniela et al[2] [1999] have studied the computational and experimental data of tube erosion in a fluidised bed and simulated the work with CFX code having computational model of hydrodynamics and Finnie model of erosion. The results predicted that most of wear occurs around the bottom of tube at an oblique impaction angle and very low value at the top of the tube.

Manickam M. et al[3] [1999] have modelled the flow in the bifurcation duct of a power generation boiler plant. The computational fluid dynamics code was customized to determine erosion rate caused by particles that hit the duct wall. To reduce the wall duct erosion, five modifications to the duct geometry were tested using the CFD model. The focus of these modifications have been used to improve particle flow characteristics to mitigate the erosion of the walls of the duct by using extended trailing edged or setting up more baffles in the central zone where the particle traffic is intense.

Anders Sellgren et al[5][1999] have studied the effects of non-Newtonian mineral suspensions on the performance of centrifugal pumps. They have investigated how the non–Newtonian rheology of some industrial suspension influences the performance of centrifugal pumps. Slurry used in this experiment is red mud associated with production of aluminium. It is observed that influence on the performance is normally small with the values of kinematic viscosity of fluids less than 0.1×10^{-3}. Also

reductions in pump head and efficiency in the best efficiency point (BEP) region was at a maximum about 10 and 20%. It has also been observed that pumping highly viscous fluids can cause large drop in efficiency.

Lee S. Y. et al[6] [2001] have discussed the application of computational fluid dynamics (CFD) methods to simulate the flow of slurry and predict the erosion rates so that an effective maintenance schedule can be developed for the filtration system of the waste treatment process. The location of the maximum erosion for the selected components is also identified. Solids content of the working fluid, the regions of high wall shear, and particle impingement with the walls were considered as major mechanisms associated with the erosion. All these tests were performed using sand-water slurry.

Gandhi B. K. et al[7] [2001] have observed that performance of pumps decreases for increase in solid concentration, particle size and specific gravity. The head and efficiency of the pump decrease with increase in solid concentration, particle size, and slurry viscosity, the decrease in the head being 2–10 percent higher than that of the efficiency. The presence of finer particles (less then 18micron) in coarser slurries substantially attenuates the loss of performance of the pump in terms of head and efficiency. At low solid concentrations less than 30 percent by weight, the increase in the pump input power is directly proportional to the specific gravity of slurry whereas the same relationship is not applicable at higher concentrations. The study on the pumps has confirmed that the additional head loss for slurries decrease with increase in the pump size.

Hawthorne H.M.[8] [2001] has conducted Coriolis tests for the evaluation of slurry erosion on different materials. Slurries consisting of glass beads of size 90- 200-micron size with 10% slurry concentration were taken and tests were performed on 1020 steel and copper at different impingement angles of 90-20 degrees. It was also observed that in slurry jet testing, most particles impact the specimen above its critical velocity resulting severe plastic deformation. In contrast, in the Coriolis test most particle impacts result in only elastic deformation or mild plastic deformation. Hence, elastic as well as plastic properties of specimen materials affect their performance in a Coriolis slurry erosion evaluation, thus the results obtained from Coriolis tests were more accurate.

Clark H. McI.[10] [2002] has investigated the effect of Particle velocity and particle size in slurry erosion. A list of factors affecting slurry erosion such as concentration of particles, Slurry flow speed (particle impact speed), particle impact angle ,particle size, particle density, hardness, friability, nature of suspending liquid, nature of slurry flow (esp. local turbulence),nature of target material were explained. It is emphasized that material loss must be measured by changes in surface profile rather than mass loss, and that the best specimen form for this analysis is a cylinder.

Zhou Weidong et al[11] [2003] have investigated the flow through a centrifugal pump impellers using computational fluid dynamics and describes the three-dimensional simulation of internal flow in three different types of centrifugal pumps A commercial three-dimensional CFX code, with a standard two-equation turbulence model was used to simulate the problem under examination . In the calculation, the finite-volume method and an unstructured grid system were used for the solution .Comparison of computational results for various types of pumps showed good agreement for the twisted-blade pumps.

Hamed Awatef A. et al[12] [2002] have observed the blade surface deterioration by erosion. A combined experimental and computational work was to investigate turbine vane and blade material surface deterioration caused by solid particle impacts. Tests were conducted in the erosion wind tunnel for coated and uncoated blade materials at various impact conditions. Surface roughness measurements obtained prior and subsequent to the erosion tests were used to characterize the change in roughness caused by erosion. Numerical simulations for the three dimensional flow field and particle trajectories through a low pressure gas turbine were employed to determine the particle impact conditions with stator vanes and rotor blades using experimentally-based particle restitution models.

Engin Tahsin et al[13] [2003] have evaluated some existing correlations to predict head degradation of centrifugal slurry pumps. A new correlation has been developed in order to predict head reductions of centrifugal pumps when handling slurries. The proposed correlation takes into account the individual effects of particle. The proposed correlation is therefore recommended for the prediction of performance factors of ‘‘small-sized’’ slurry pumps having impeller diameters lower than 850 mm.

size, particle size distribution, specific gravity and concentration of solids, and impeller exit diameter on the pump performance.

Clark H.McI[14] [2004] has studied the influence of the squeeze film in slurry erosion. A 'squeeze film' may be taken as any liquid layer separating two approaching surfaces. The presence of a squeeze film generally leads to a significant retardation of any particle closely approaching a wearing surface at any speed and may even prevent direct impact altogether. The experiments were performed in slurry pot tester. In addition to this it is has also found that if the Reynolds number (i.e. velocity or mass) of the approaching particles is low enough, penetration of the squeeze film on rebound or even approach may not be possible, resulting in particle entrapment at the target surface and a change in erosion mechanism. He observed that small particles (less then100 micron) and concentrated slurries were especially liable to behave in this way.

Gandhi B. K. et al[15] [2004] have developed a methodology to determine the nominal particle size of multi-sized particulate slurry for estimation of mass loss due to the erosion wear. The effect of presence of finer particles (less then 75 micron) in relatively coarse particulate slurry has also been studied. They have observed that addition of particles finer than 75 micron in narrow-size or multi-sized slurries reduce the erosion wear. In addition, the effective particle size for narrow-size particulate slurries can be taken as the mean size whereas the weighted mass particle size seems to be a better choice for multi-sized particulate slurries. The reductions in erosion wear due to addition of fine particles decreases with increase in the concentration of coarse size particles.

Rajesh J. John et al[16] [2004] have carried out experiments on the effect of impinging velocity on the erosive wear behaviour of polyamides. The impact angles were 30 and 60 degrees at two impact velocities (80 and 140 m/s). Silica sand is used as an erodent. Surface blackening at the impact zone was observed for all the materials at normal impact and at both the impact velocities. At normal impact and at lower impinging velocity (i.e. 80 m/s), a mass gain in the initial period was observed for all the materials except amorphous. The extent of increase in wear, however, depended on the materials and the angle of impact. The velocity effect was more prominent at the oblique angle of impact.

Wang Yao et al[17] [2005] have designed an experimental system for wear assessment of slurry pumps. Slurry density of 1450 *kg/m*3 has been taken. The wear patterns on the suction liner, impeller and volute casing were shown. Two locations were found to be most easily worn in impellers: the root of each vane and the area on the back shroud close to the suction side of the vane root.

Tian Harry H. et al[18] [2005] have observed the erosive wear of some metallic materials such as high chromium white iron and aluminium alloy using Coriolis wear testing approach. In the present study, the correlation between wear rate and particle size on the tested materials is discussed. Factors, which should be considered in wear modelling and prediction, have also been addressed. It can be seen that larger solids particles resulted in higher mass loss in all test materials. Although the wear rates at smaller particle sizes were relatively close within each material group, the wear rate difference was significantly widened with larger particle sizes. The tested high-Cr white irons showed a wear resistance some 27–140 times higher than that of the aluminium alloys in the Coriolis test conditions Both flow rate and solids concentration of slurry affected the wear results of the test materials. The higher the flow rate, the higher the wear rate of test materials.

Asuaje Miguel et al[19] [2005] have simulated the 3D-CFD model of the impeller and volute of a centrifugal pump using CFX codes. A sensitivity analysis regarding grid quality and turbulence models were also performed. A procedure for designing the volute, the non-structured grid generation and the interface flow passage between the impeller and volute were discussed. The flow simulations were carried out for several impeller blades and volute tongue relative positions. It was observed that the numerical solution is stabilized with grids containing more than 40 000 nodes. Also A non uniform pressure distribution develops at the impeller periphery as a function of the pump flow rate, causes a fluctuating radial thrust of significant amplitude.

Tian Harry H. et al[20] [2005] have experimented on Coriolis wear testing. Wear coefficients (or specific energy coefficients) have been determined for different slurry conditions over a large range of particle sizes. Among the test materials, the harder Cr–Mo white iron alloy demonstrated the best wear resistance under slurry testing conditions. It is also observed that Coriolis wear testing is an excellent approach to simulate the erosive wear condition within a slurry pump. Beside particle sizes, other

particle properties such as particle shape and size distribution also exhibited significant effect on the values of wear coefficients. Silica sand and copper ore slurries were used as examples. The relationship between linear wear rate and solid particles was also shown.

Das S K et al[21] [2006] have developed a mathematical model embodying the mechanisms of erosion on behaviour, to predict erosion rate of coal-fired boiler components at different temperatures. Various grades of steels used in fabrication of boiler components and published data pertaining to boiler fly ash have been used for the modelling. The model incorporates high temperature tensile properties of the target metal surface at room and elevated temperatures and has been implemented in an user-interactive in-house computer code, to predict the erosion rates of various grades of steel. The model is calibrated with plant and experimental data generated from a high temperature air-jet erosion-testing facility

Li Ping et al[22] [2006] have observed the failure analysis of the impeller used in zinc hydrometallurgy process. Failure analysis revealed that an improper austenite/ferrite ratio of duplex stainless steel (DSS) material resulting from too high nitrogen content was primarily responsible for the rapid failure of the impeller. It was also observed that nitrogen content had a significant effect on austenite/ferrite ratio of duplex steel. The result of simulated corrosive wear test indicated that duplex stainless steel possessing almost equal ferrite and austenite volume showed better corrosive wear resistance.

Roudnev et al[23] [2007] have observed the erosion wear of casing of slurry pumps and predicted the accurate location of maximum erosion through CFD simulations and experimental data. All 3D simulations predicted similar wear rate magnitudes. It is being estimated that area nearer to upper part of volute casing experiences maximum wear. CFD multiphase simulation using the Eulerian-Eulerian approach is being applied to determine the velocity fields and solid concentration in the centrifugal pump.

Shah Subhash N. et al[24] [2007] have conducted experiments to visualize the effect of slurry flow rate on the erosion of coiled tubing. Erosion rate has been investigated as a function of flow rate, slurry concentration, solid particles size and density, and fluid viscosity. This study utilizes both experimental tests and CFD simulations to

investigate erosion by fracturing fluids. In hydraulic fracturing, the fracturing fluid is pumped at high enough rates to overcome the tensile strength of the rock and thus break the formation open. The slurry is pumped through 6 cm coiled tubing at rates from 1.43 to 1.91 cubic m^3/min. CFD simulations have been conducted by utilizing erosion prediction and particle tracking modules in a commercial CFD code FLUENT.

Desale Girish R. et al[25] [2007] have conducted experiments to visualize the effect of slurry erosion on ductile materials under normal impact condition. These tests were being done in slurry pot tester. It is being observed that wear depends upon hardness of target material and hardness of solid particles. The various ductile materials tested were copper, mild steel brass etc. The erodent materials used were quartz, alumina, and silicon carbide. Experiments were performed at 3m/s velocity and 10 percentage by weight concentration of 550 micron size particles for combination of different erodent and target materials at normal impact condition.

Kergourlay G et al[26] [2007] have observed the influence of adding splitter blades on the performance of a hydraulic centrifugal pump. Velocity and pressure fields were computed using unsteady Reynolds-averaged Navier- Stokes (URANS) approach at different flow rates. The sliding mesh method is used to model the rotor zone motion in order to simulate the impeller-volute casing interaction. The flow morphology analysis shows that, when adding splitter blades to the impeller, the impeller periphery velocities and pressures become more homogeneous. The pressure fluctuations were measured at four locations at the BEP using dynamic pressure sensors.

Cheah K. Wet et al[27] [2007] have performed the numerical simulation on impeller of centrifugal pump with six twisted blades. The result shows that the impeller passage flow at design point is quite smooth and follows the curvature of the blade. However, flow separation is observed at the leading edge due to non tangential inflow condition. For the pressure distribution, the pressure increases gradually along stream-wise direction in the impeller passages. When the centrifugal pump is operating under off-design flow rate condition, unsteady flow developed in the impeller passage and the volute casing. Different flow rates were specified at inlet boundary to predict the characteristics of the pump.

Feng Jianjun et al[28] [2007] have conducted numerical simulations on impeller-diffuser interactions in radial diffuser pumps to investigate the unsteady flow, and more attention is paid to pressure fluctuations on the blade and vane surfaces Computational results show that a jet-wake flow structure is observed at the impeller outlet. The biggest pressure fluctuation on the blade is found to occur at the impeller trailing edge, on the pressure side near the impeller trailing edge, and at the diffuser vane leading edge, independent of the flow rate, radial gap, and blade number configuration. All of the flow rate, blade number configuration, and radial gap influence significantly the pressure fluctuation and associated unsteady effects in the diffuser pump.

MOTIVATION OF THE PRESENT WORK

Slurry erosion is a crucial problem in many industrial applications, due to impingement of solid particles being suspended in the fluids flowing at high velocity. It affects both the initial cost and life of the component. The service life of equipment handling solid –liquid mixture can be increased by reducing the erosion wear. It is therefore necessary to study erosion wear systematically, so that efforts can be made to minimize the wear during design stage.

The experimental testing on centrifugal pump is very complex and working condition specific such as variations in different types of slurries, chemical and mechanical properties. Also, today the numerical simulation is viewed as a new third dimension in engineering predictions. The other two dimensions are pure experiments and pure theory. The use of CFD for computation provides an efficient tool for simulation of the flow field characteristics inside the turbo machinery. These two factors namely, the limited experimental data available related the erosion wear on centrifugal slurry pump and the application of CFD to analyze the erosion wear characteristics inside the pump.

Following are the objectives of the present work

1) To design the impeller blade and volute casing of centrifugal pump for given data.

2) To develop a generalized program for design of centrifugal slurry pump by using C++.

3) To simulate the erosion wear of impellor blades by using a CFD software.

4) To study the affecting parameters in the erosion wear on impeller blades.

CHAPTER 3

DESIGN OF CENTRIFUGAL PUMP

Before a pump can be selected or prototype designed, its application must be clearly defined. As pump requirements must match system characteristics, analysis of overall system is necessary in which the pump is to be installed .There are a lot of parameters on which design of pump depends. For this design, head flow rate, speed and overall efficiency has been taken as input.

The flow through the impeller is assumed to be resolved into two parts

a) Through flow with relative velocity assuming the impeller to be stationary

b) Rotational flow

The first part helps to design runner passages after assuming through flow velocity. The second part helps to fix up outer diameter of impeller because this is mainly responsible for developing the head required. The following procedure[33] is followed for design of centrifugal pump impeller.

3.1 INPUT DATA

Head (H) = 14.5 m

Flow Rate (Q) = 0.016 m^3/sec

Speed (N) = 1450 rpm

3.2 DESIGN OF IMPELLER:

3.2.1. Specific Speed

Specific speed of the pump is computed based on the power as well as discharge; different authors expressed the design parameter as function of specific speed.

$$N_s = \frac{N\sqrt{Q}}{H^{0.75}} \qquad (3.1)$$

Where

N = Speed at which pump shaft rotates=1450 rpm.

Q = Flow Rate =0.016 m^3 / sec

H = Head =14.5 m.

$$N_s = 24.683 \text{ rpm}$$

3.2.2. Input Power and Shaft Power

$$\text{Output Power } P_0 = \rho gQH \tag{3.2}$$

$$\text{Input power } P_{in,} = \left(\frac{\rho gQH}{745\ \eta_0}\right) \tag{3.3}$$

Where

g=Acceleration due to gravity

ρ=Density of the fluid

Overall efficiency is taken from the graph, and is taken equal to 0.75 percent. Input power required 15% more because of bearing and transmission losses.

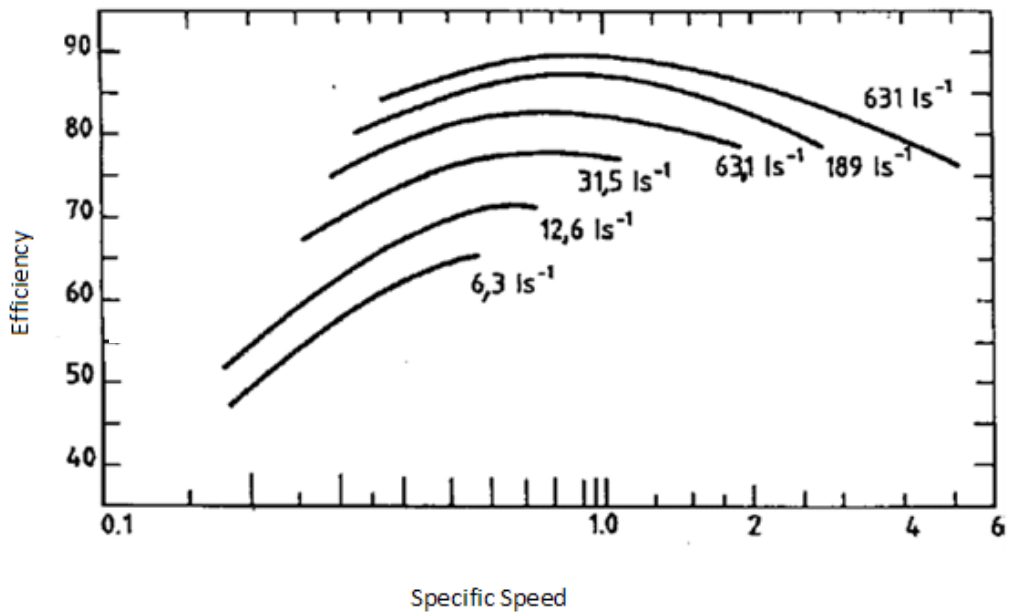

Fig 3.1: Variation of Efficiency with Specific Speed[33]

$$\text{Calculated input power } P_{in} = \frac{1000x9.81x0.016x14.5}{745x0.46}$$

$= 6.641$ HP

Shaft power $P_{sh} = 1.15\ P_{in}$

Shaft Power $P_{sh} = 1.15 \times 6.641$

$= 7.6373$ HP

The relationship between hydraulic and overall efficiency[33] is shown by eq. (3.4).

$$(1-\eta_h) = 0.66(1-\eta_o) \tag{3.4}$$

Hydraulic Efficiency, $\eta_h = 0.6436$

Overall Efficiency, $\eta_o = \eta_h \times \eta_v \times \eta_m$ (3.5)

Mechanical Efficiency $\eta_m = 0.7768$

3.2.3. Shaft Diameter (d_{sh})

Torque transmitted by the shaft

$$T = \left(\frac{P_{sh} \times 60 \times 750}{2\pi N}\right) \text{ N m} \tag{3.6}$$

Putting the values of Psh and N in the above equation we get

$T = 37472.5$ N m

Shaft Diameter can be calculated from the given equation(3.7)

$$d_{sh} = \left(\frac{16T}{\pi F_s}\right)^{\frac{1}{3}} \tag{3.7}$$

$d_{sh} = 0.019689$ m

Where

F_s = 25 MPa, Stress depending on the material constant

For the present problem the shaft is assumed to be made of steel with an allowable shear stress of 25 MPa

3.2.4 Hub Diameter (D_{hb})

$$D_{hb} = (1.2 \text{ to } 1.3)\ Dsh \qquad (3.9)$$

For given data D_{hb} = 1.2 x 0.019689

= 0.023627 m

3.2.5. Design of Suction Passage

1) Discharge through the impeller

$$Q' = Q + \Delta Q \qquad (3.10)$$

$$Q' = 0.016+0.016*0.08$$

$$Q' = 0.01728 \text{ m3/sec}$$

Where

Q = Flow rate at inlet

Q' = Flow rate at outlet

ΔQ = Mass flow rate losses or volumetric losses

2) Calculation of axial velocity at entry of impeller

For the given specific speed, assume the values of dimensionless parameters

$$C_A = 0.152\left(\frac{\sigma^2 \tan^2 \beta_3}{\tau^2 K}\right)^{\frac{1}{3}} \left(N^2 Q'\right)^{\frac{1}{3}} \qquad (3.11)$$

$$C_A = 2.5469 \text{ m/s}$$

Where

C_A = Axial velocity at entry of impeller.

Thoma cavitation factor σ = 1.1 (Varies from 0.9 – 1.1)[33]

Circulation losses τ = 1.05 (Varies from1.05 – 1.1)[33]

Constant K = 0.84 (Varies from 0.75 – 0.85) [33]

Relative inlet angle at hub β_3 = 17.5

3) Calculation of eye diameter (D_e)

$$D_e = \sqrt{\frac{4Q'}{\pi K C_A}} \quad (3.12)$$

D_e = 0.1014 m

D_1 = 0.95 * D_e

= 0. 09633 m

C_0 = 1.05 * C_A

= 2.6742 m/s

C_1 = 1.1 * C_0

= 2.9416 m/s

Where

C_1 = Absolute Velocity at inlet of the blade

C_0 = Absolute Velocity at eye of the blade.

D_1 = Diameter at the inlet of the blade.

4) Breadth of the blade at the inlet (b_1)

$$b_1 = \frac{Q'}{\pi D_1 C_1} \quad (3.13)$$

= 0.02135 m

5) Blade velocity at inlet (u_1)

$$u_1 = \frac{\pi D_1 N}{60} \quad (3.14)$$

$$= 7.3135 \text{ m/s}$$

6) Blade inlet angle (β_1)

$$\beta_1 = \tan^{-1}\left(\frac{C_1}{u_1}\right) \quad (3.15)$$

$$= 21.91°$$

2.6 Design of discharge passage

The governing equation for solution to outlet end dimensions is the Euler's equation. For rotation free inlet this may be written as:

$$H_r = \frac{u_2^2}{g} - \frac{u_2 C_{2m}}{g}\cot\beta_2 \quad (3.16)$$

Where

H_r = Total head generated

C_{2m} = Meridional flow velocity inside impeller

g = Acceleration due to gravity

u_2 = Blade velocity at outlet

The left hand side of this equation is related to total head generated as given below.

$$H_r = (1+p)\frac{H}{\eta_h} \quad (3.17)$$

$$= (1+0.32)* 14.5/0.6436$$

$$= 29.7389 \text{ m}$$

Where

η_h = 0.6436 (Calculated in equation (3.4))

p = 0.32 (Varies from 0.28 to 0.35)[33]

p is Pfleiderer's coefficient, a factor relating the difference between the imaginary and ideal conditions inside the pump.

The value of meridional flow velocity inside an impeller does not vary much and can be kept constant. However its value is generally somewhat lower than that at the suction end and so assume

$$C_{2m} = 0.9 * C_{1m} \quad (3.18)$$

$$= 0.9 * 2.9416$$

$$= 2.6474 \text{ m/sec}$$

Where

C_{1m} = Meridional Flow Velocity at suction end

β_2 (Outlet Blade Angle) is assumed to be as 26° (varies from 20°-26°)[32]

Substituting these values in Euler's equation (3.16)

$$29.7389 = \frac{u_2^2}{9.81} - \frac{u_2 \times 2.6474}{9.81} \cot 26^0$$

Blade velocity at outlet

u_2 = 20.0085 m/sec

Outer Diameter of impeller

$$D_2 = \frac{u_2 \times 60}{\pi N} \quad (3.19)$$

D_2 = 0.2635 m

3.2.7. Number of Blades (Z)

$$Z = 2\pi \frac{D_1 + D_2}{D_2 - D_1} \sin 22 \quad (3.20)$$

$$= 5.06 \approx 5$$

3.2.8 Width of Blade at Outlet (B_2)

$$B_2 = \frac{Q'}{\pi D_2 C_{2m}}$$

$$= 0.0078848 \text{ m}$$

3.2.9. NET POSITIVE SUCTION HEAD (NPSH)

$$\Delta H = \lambda_1 \frac{W_2^2}{2g} + \lambda_2 \frac{C_2^2}{2g} \quad (3.21)$$

Take, $\lambda_1 = 0.3$,

$\lambda_2 = 1.2$

Where λ_1 is the constant considering losses in the impeller whose value is dependent on the machine performance[32], λ_2 is losses in suction pipe.

$$W_2 = \frac{C_2}{\sin \beta_2} \quad (3.22)$$

$$= 8.8930$$

Where

$W_2 =$ Relative velocity at the eye of the impeller

After substituting $\Delta H = 1.6466$ m

The results of the analytical work have been summarized in table 3.1

Table 3.1: Summary of Design data for design of centrifugal pump

No.	Design Parameter	Values
1	Specific speed of the pump	24.683
2	Hydraulic efficiency of the pump	00.6436
3	Mechanical Efficiency of the pump	0.776
4	Shaft power of the pump	7.6373 HP
5	Torque transmitted by the shaft	37472.5 N-m
6	Diameter of the Shaft	0.019689 m
7	Axial velocity	2.5469 m/s
8	Eye diameter	0. 09633 m
9	Inlet blade diameter	0.0963058 m
10	Hub diameter	0.0236283 m
11	Width at inlet	0.021342 m
12	Inlet blade velocity	7.3115 m/s
13	Outlet blade velocity	20.0085 m/sec
14	Outlet diameter of blade	0.2635 m
15	Number of blades	5
16	Width at outlet of blade	0.0078848 m
17	NPSH	1.6466

CHAPTER 4

INTRODUCTION TO COMPUTATIONAL FLUID DYANAMICS

4.1 INTRODUCTION TO CFD

Computational fluid dynamics (CFD) is one of the branches of fluid mechanics that uses numerical methods and algorithms to solve and analyze problems that involve fluid flows. CFD has become an indispensable tool in the design, development, evaluation and refinement of new industrial equipment and processes. The use of CFD reduces the development cost of new products and cuts the time to market of these products. CFD have applications in

1. Aerospace,

2. Automotive Design,

3. Electronics,

4. Food, Chemical, and Material Processing,

5. Power Generation

Computational Fluid Dynamics (CFD) has become an integral part of the engineering design cycle. Whether it is used to design industrial mixing tanks, aerospace components, or used to simulate transient flow phenomenon in pumps and turbines. CFD analyses reduce development time and increase the reliability of prototype designs. CFD simulations can be used to model fluid flows over a wide range of physical scales. The fundamental basis of any CFD problem is the Navier-Stokes equations, which define any single-phase fluid flow. It works by solving the equations of fluid flow (in a special form) over a region of interest, with specified (known) conditions on the boundary of that region.

4.2 HISTORY OF CFD

Computers have been used to solve fluid flow problems for many years. Numerous programs have been written to solve either specific problems, or specific classes of problems. From the mid-1970's, the complex mathematics required to generalize the algorithms began to be understood, and general purpose CFD solvers were developed. These began to appear in the early 1980's and required what were then very powerful computers, as well as an in-depth knowledge of fluid dynamics, and large amounts of time to set up simulations. Consequently, CFD is a tool used almost exclusively in research.

Recent advances in computing power, together with powerful graphics and interactive 3D manipulation of models have made the process of creating a CFD model and analyzing results much less labour intensive, reducing time and, hence, cost. Advanced solvers contain algorithms which enable robust solutions of the flow field in a reasonable time. As a result of these factors, Computational Fluid Dynamics is now an established industrial design tool, helping to reduce design time scales and improve processes throughout the engineering world. CFD provides a cost-effective and accurate alternative to scale model testing with variations on the simulation being performed quickly offering obvious advantages.

4.3 CFD METHODOLOGY

4.3.1 Initial design

In order to obtain better design in CFD, following procedure is applied so that fluid flow can easily be modelled. Initial design of the model is a planning decision and the geometry is generated depending on these initial design considerations, using either CFD modelling tools or other Design tools.

4.3.2 Geometry generation

The first task to accomplish in a numerical flow simulation is the definition of the geometry, followed by the grid generation. This step is the most important step for the study of an isolated impeller assuming an axis symmetric flow simplifies the domain to a single blade passage.

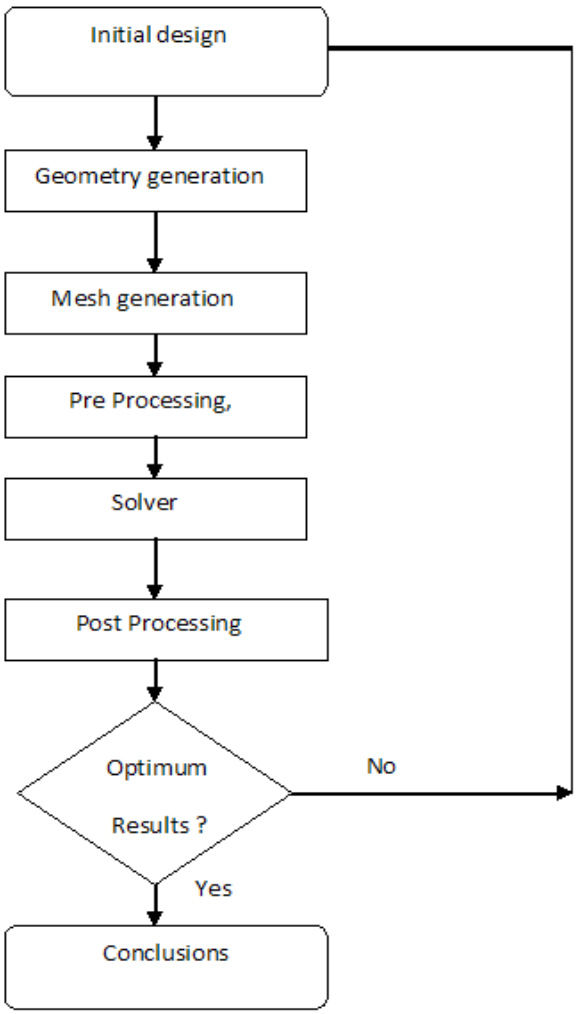

.

Figure 4.1: Flow chart showing CFD solving methodology

The geometry of design needs to be created from the initial design. Any modelling software can be used for modelling and then shifted to other simulation software for analysis purposes.

4.3.3 Mesh generation

Mesh generation (Gridding) is the process of subdividing a region to be modelled into a set of small control volumes. Associated with each control volume there will be one or more values of the dependent flow variables (e.g., velocity, pressure, temperature, etc.) Usually these represent some type of locally averaged values. Numerical algorithms representing approximations to the conservation laws of mass, momentum and energy are then used to compute these variables in each control volume.

Meshing is a method to define and break up the model into small elements. In general, a finite element model is defined by a mesh network, which is made up of the geometric arrangement of elements and nodes. Nodes represent points at which features such as displacements are calculated. Elements are bounded by sets of nodes, and define localized mass and stiffness properties of the model. Elements are also defined by mesh numbers, which allow references to be made to corresponding deflections, stresses, pressures, temperatures at specific model locations. The traditional method of mesh generation is block-structure (multi-block) mesh generation. The block-structure approach is simple and efficient technique of mesh generation.

4.3.3.1 Topology

The topology is a structure of blocks that acts as a framework for positioning mesh elements. Topology blocks represent sections of the mesh that contain a regular pattern of hexahedral (hex) elements. They are laid out adjacent to each other without overlap or gaps, with shared edges and corners between adjacent blocks, such that the entire domain is filled. By using topology blocks to control the placement of hex elements, a valid hexmesh can be generated to fill a domain of arbitrary shape. The topology is invariant from hub to shroud and is viewed/edited on 2-D layers which are located at various spanwise stations. The topology blocks can be arranged in a regular (structured) pattern, an irregular (unstructured) pattern, or in a pattern consisting of structured patches and unstructured patches. The choice of which approach should be followed should be based on whichever method minimizes the maximum skew of the topology blocks, since the skew in the hex elements of the mesh is directly related. The topology should then be investigated at various layers (especially the hub and shroud layers) to check its quality since the mesh quality is directly dependent on topology. Topology blocks generally contain the same number of mesh elements along each side. The mesh elements vary in size across topology blocks in a way that produces a smooth transition within and between blocks. This is accomplished by shifting the nodes toward, or away from, certain block edges.

There are basically 3 types of topologies which is generally used

1) H-Grid
2) J-Grid

3) O-Grid

In actual conditions, a combination of these topologies is used. An O-Grid is a topology that forms a continuous loop around the blade profile. Using an O-Grid around the blade yields excellent boundary layer resolution and near-orthogonal elements on the blade.

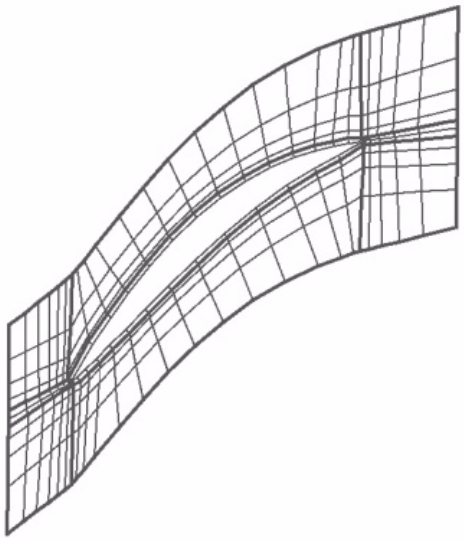

Figure 4.2 Topology of Type H

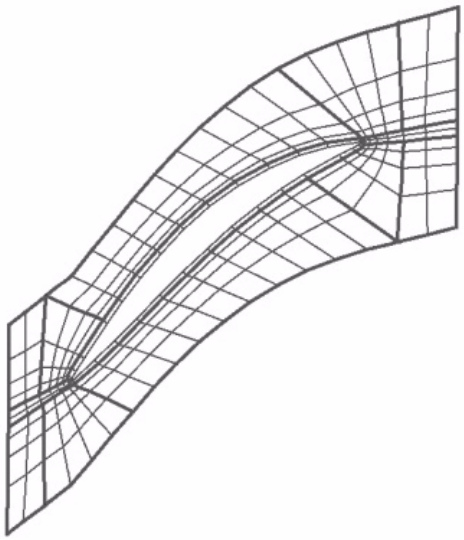

Figure 4.3 Topology of Type J

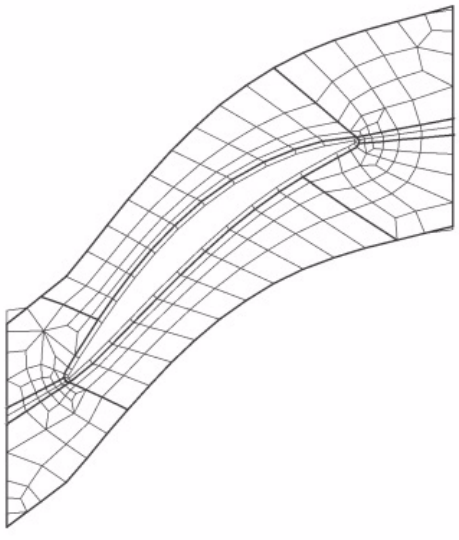

Figure 4.4 Topology of type H-Grid Dominant

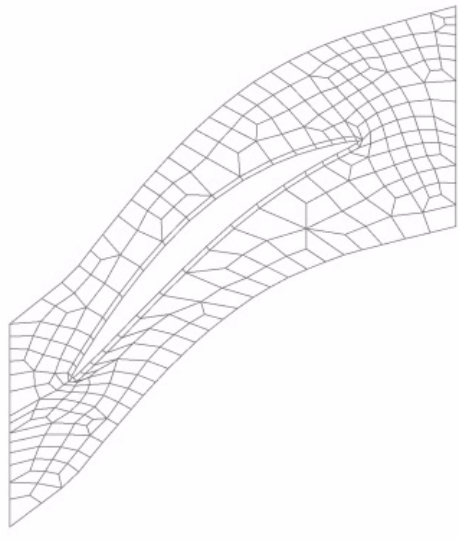

Figure 4.5 Topology of Type Automatic

H-Grid Dominant adds some topology blocks in a structured manner around an optional embedded O-Grid that surrounds the blade (as for a topology of type H-Grid), then completes the mesh by adding topology blocks in an unstructured manner. The structured blocks extend upstream of the leading edge, downstream of the trailing edge, and from the blade to the periodic surfaces. Automatic adds topology blocks in an unstructured isotropic manner around an optional O-Grid that surrounds the blade.

4.3.4 Preprocessing

4.3.4.1 Boundary condition

The first step in Pre-processing is setting up the boundary conditions. Boundary condition will be different for each type of problem. In Cartesian and cylindrical-polar coordinates, the location of boundary features (inlets, outlets, blockages, etc) can be linked to named 'objects' defined during the grid-generation procedure. This obviates the need to enter the coordinates twice: once when defining the grid, and again when specifying boundary conditions.

If an 'object' is subsequently repositioned or re-sized, then the boundary condition is also changed automatically. If an object is deleted, any associated boundary-conditions will also be deleted without further instructions from the user. If a new 'object' is created by copying an existing one, the boundary conditions are not automatically copied, but a new boundary condition may be linked to the new object.

In low speed and incompressible flows, disturbances introduced at an outflow boundary can have an effect on the entire computational region. As a general rule, a physically meaningful boundary condition, such as a specified pressure condition, should be used at out flow boundaries whenever possible. Generally, a pressure condition cannot be used at a boundary where velocities are also specified, because velocities are influenced by pressure gradients. The only exception is when pressures are necessary to specify the fluid properties, e.g., density crossing a boundary through an equation of state.

The inlet condition for velocity and temperature can be specified using profile of grid. The turbulent kinetic energy (k) and its dissipations rate can be calculated from the value of turbulence intensity specified in the inlet.

4.3.4.2 Turbulence models

Turbulence consists of fluctuations in the flow field in time and space. It is a complex process, mainly because it is three dimensional, unsteady and consists of many scales. It can have a significant effect on the characteristics of the flow. Turbulence occurs when the inertia forces in the fluid become significant compared to viscous forces, and is characterized by a high Reynolds Number. In general, the Navier-Stokes equations describe both laminar and turbulent flows without the need for additional information. However, turbulent flows at realistic Reynolds numbers span a large range of turbulent length and time scales, and would generally involve length scales much smaller than the smallest finite volume mesh, which can be practically used in a numerical analysis. The Direct Numerical Simulation (DNS) of these flows would require computing power which is many orders of magnitude higher than available in the foreseeable future.

Turbulence models are used to predict the effects of turbulence in fluid flow without resolving all scales of the smallest turbulent fluctuations. A number of models have been developed that can be used to approximate turbulence based on the Reynolds Averaged Navier-Stokes (RANS) equations. Some have very specific applications, while others can be applied to a wider class of flows with a reasonable degree of confidence. One of the main problems in turbulence modelling is the accurate prediction of flow separation from a smooth surface. Standard two-equation turbulence models often fail to predict the onset and the amount of flow separation under adverse pressure gradient conditions. This is an important phenomenon in many technical applications, particularly for airplane aerodynamics since the characteristics of a plane are controlled by the flow separation from the wing.

In general, turbulence models based on the equation predict the onset of separation too late and under-predict the amount of separation later on. This is problematic, as this behaviour gives an overly optimistic performance characteristic for an airfoil. The prediction is therefore not on the conservative side from an engineering stand-point. The models developed to solve this problem have shown a significantly more accurate prediction of separation in a number of test cases and in industrial applications. Separation prediction is important in many technical applications both for internal and external flows.

a) k-ε turbulence model

One of the most prominent turbulence models, the $k-\varepsilon$ (k-epsilon) model, has been implemented in most general purpose CFD codes and is considered the industry standard model. It has proven to be stable and numerically robust and has a well established regime of predictive capability. For general purpose simulations, the model offers a good compromise in terms of accuracy and robustness.

Within ANSYS CFX, the $k-\varepsilon$ turbulence model uses the scalable wall-function approach to improve robustness and accuracy when the near-wall mesh is very fine. The scalable wall functions allow solution on arbitrarily fine near wall grids, which is a significant improvement over standard wall functions. While standard two-equation models, provide good predictions for many flows of engineering interest k is the turbulence kinetic energy and is defined as the variance of the fluctuations in velocity. ε is the turbulence eddy dissipation (the rate at which the velocity fluctuations dissipate), and has dimensions of per unit time. The k-ε model introduces two new variables into the system of equations.

The continuity equation is then:

$$\frac{\partial \rho}{\partial t} + \nabla \bullet (\rho U) = 0 \tag{4.1}$$

and the momentum equation becomes

$$\frac{\partial \rho U}{\partial t} + \nabla \bullet (\rho U \otimes U) - \nabla \bullet (\mu_{eff} \nabla U) = -\nabla p' + \nabla \bullet (\mu_{eff} \nabla U)^T + B \tag{4.2}$$

where

B = Sum of body forces,

μ_{eff} = Effective viscosity accounting for turbulence,

ρ = Modified pressure

b*) k-ω* turbulence model

One of the advantages of the $k-\omega$ formulation is the near wall treatment for low-Reynolds number computations. The model does not involve the complex non-linear damping functions required for the $k-\varepsilon$ model and is therefore more accurate and more robust The models assumes that the turbulence viscosity is linked to the turbulence kinetic energy and turbulent frequency via the relation:

$$\mu_t = \frac{k}{w} \tag{4.3}$$

Where

μ_t = Turbulence viscosity

k = Turbulence kinetic energy and is defined as the variance of the fluctuations in velocity

w=Turbulence frequency

c) Shear stress transport (SST) model

The Shear-Stress-Transport (SST) model is designed to give highly accurate predictions of the onset and the amount of flow separation under adverse pressure gradients by the inclusion of transport effects into the formulation of the eddy-viscosity. This results in a major improvement in terms of flow separation predictions. The superior performance of this model has been demonstrated in a large number of validation studies [38]. $k-\varepsilon$ model do not account for the transport of the turbulent shear stress.The SST model is recommended for high accuracy boundary layer simulations.The proper transport behavior can be obtained by a limiter to the formulation of the eddy-viscosity

$$v_t = \frac{a_{1k}}{\max(a_1\omega, SF_2)} \tag{4.4}$$

Where

$v_t = \mu_t / \rho$

μ_t = Turbulent viscosity

ρ = Density

F_2 = Blending function which restricts the limiter to the wall

S = Strain rate.

These models require the distance of a node to the nearest wall for performing the blending between $k-\varepsilon$ and $k-\omega$ turbulence models. Blending functions are used for transformation of the one turbulence model to another

4.3.4.3 Multiphase flow

Multiphase flow is a flow in which more than one fluid is present. In general, the fluids consist of different chemical species, e.g., air-water. In some applications, they may represent different thermodynamic phases of the same species, e.g., steam-water. It is important to distinguish between multi component and multiphase flow. A Multi component fluid is assumed to consist of a mixture of chemical species which are mixed at the molecular level. In this case, single mean velocity and temperature fields, etc., are solved for the fluid. Examples are gaseous mixtures, and solutes in liquids. The fluids in a multiphase flow are assumed to be mixed at macroscopic length scales, much larger than molecular. Examples are gas bubbles in liquid, liquid droplets in a gas or in another immiscible liquid, etc. In this case, it is necessary to solve for different velocity and temperature fields, etc., for each fluid.

a) Basics of particle transport model

The Particle model for interfacial transfer between two phases assumes that one of the phases is continuous (α phase) and the other is dispersed (β phase). The surface area per unit volume is then calculated by assuming that β phase is present as spherical particles of Mean Diameter d_β.Using this model, the inter phase contact area is:

$$A_{\alpha\beta} = 6r_\beta / d_\beta \tag{4.5}$$

Where

$A_{\alpha\beta}$ = Surface area per unit volume

d_{β} = Mean Diameter of Spherical particles

r_{β} = Minimum volume fraction

Particle transport modelling is a type of multiphase model, where particulates are tracked through the flow in a Lagrangian way. The full particulate phase is modelled by just a sample of individual particles. The tracking is carried out by forming a set of ordinary differential equations in time for each particle, consisting of equations for position, velocity, temperature, and masses of species. These equations are then integrated using a simple integration method to calculate the behaviour of the particles as they traverse the flow domain. The following section describes the methodology used to track the particles.

b) Lagrangian tracking implementation

Within the particle transport model, the total flow of the particle phase is modelled by tracking a small number of particles through the continuum fluid. The particles could be solid particles, drops or bubbles. The application of Lagrangian tracking in ANSYS CFX involves the integration of particle paths through the discretized domain. Individual particles are tracked from their injection point until they escape the domain or some integration limit criterion is met. Each particle is injected, in turn, to obtain an average of all particle tracks and to generate source terms to the fluid mass, momentum and energy equations. Because each particle is tracked from its injection point to final destination, the tracking procedure is applicable to steady state flow analysis. The following section describes the methodology used to track the particles. The particle displacement is calculated using forward Euler integration of the particle velocity over time step.

$$x_i^n = x_i^o + v_{pi}^o \delta t \tag{4.6}$$

Where

superscripts *o* and *n* refer to old and new values respectively

v_{pi} = Particle velocity.

δt = Time Step

In forward integration, the particle velocity calculated at the start of the time step is assumed to prevail over the entire step. At the end of the time step, the new particle velocity is calculated using the analytical solution.

$$v_p = v_f + (v_p^o - v_f)\exp(-\delta t / \tau) + \tau F_{all}(1 - \exp(\delta t / \tau)) \quad 4.7)$$

In the calculation of all the forces, many fluid variables, such as density, viscosity and velocity are needed at the position of the particle. These variables are obtained accurately by calculating the element in which the particle is travelling, calculating the computational position within the element.

4.3.4.4 Basic erosion model

a) Model of Finnie

The wear of a wall due to the erosive effect of particle impacts is a complex function of particle impact, particle and wall properties. For nearly all metals, erosion is found to vary with impact angle and velocity according to the relationship

$$E = kV_P^n f(\gamma) \quad (4.8)$$

Where

E = dimensionless mass

V_p =particle impact velocity

$f(\gamma)$ = a dimensionless function of the impact angle

The impact angle is the angle in radians between the approaching particle track and the wall. The value of the exponent is generally in the range 2.3 to 2.5 for metals. Finnie's model of erosive wear relates the rate of wear to the rate of kinetic energy of impact of particles on the surface, using $n = 2$

$$f(\gamma) = 1/3\cos^2\gamma \qquad \text{if } \tan\lambda > 1/3 \quad (4.9)$$

$$f(\gamma) = \sin(2\lambda) - 3\sin^2\gamma \qquad \text{if } \tan\lambda \le 1/3 \quad (4.10)$$

b) Model of Tabakoff and Grant

In the erosion model of Tabakoff and Grant, the erosion rate E is determined from the following relation:

$$E = k_1 f(\gamma) V_P^2 \cos^2 \gamma [1 - R_T^2] + f(V_{PN}) \tag{4.11}$$

$$f(\gamma) = \left[1 + k_2 k_{12} \sin\left(\gamma \frac{\pi/2}{\gamma_0} \right) \right]^2 \tag{4.12}$$

$$R_T = 1 - k_4 V_P \sin\gamma \tag{4.13}$$

$$f(V_{PN}) = k_3 (V_P \sin\gamma)^4 \tag{4.14}$$

$$k_2 = \begin{Bmatrix} 1.0 & if\ \gamma \le 2\gamma_0 \\ 0.0 & if\ \gamma > 2\gamma_0 \end{Bmatrix} \tag{4.15}$$

Where

E= Dimensionless mass (mass of eroded wall material divided by the mass of particle)

V_p= Particle impact velocity

γ = Impact angle in radians between the approaching particle track and the wall,

γ_0 =Angle of maximum erosion,

k_1, k_2, k_3, k_4, k_{12} are model constants which depend upon particle per wall material combination.

Restitution Coefficient

Restitution behaviour is a measure of the momentum lost by the particle at impact as such and it corresponds to the work done on the target surface, which, in turn, is a measure of the extent of erosion suffered by the material of the target surface. The

velocity coefficients of restitution depend upon the hardness of the target material, the density of the particle and the impact velocity.

4.3.5 Solver

Navier-Stokes Equation

The set of equations which describe the processes of momentum, heat and mass transfer are known as the Navier-Stokes equations. These partial differential equations were derived in the early nineteenth century and have no known general analytical solution but can be discretized and solved numerically. Equations describing other processes, such as combustion, can also be solved in conjunction with the Navier-Stokes equations. Often, an approximating model is used to derive these additional equations, turbulence models being a particularly important example. There are a number of different solution methods which are used in CFD codes. The most common, is known as the finite volume technique. In this technique, the region of interest is divided into small sub-regions, called control volumes. The equations are discretized and solved iteratively for each control volume. As a result, an approximation of the value of each variable at specific points throughout the domain can be obtained. In this way, one derives a full picture of the behaviour of the flow.

The Navier-Stokes equations, named after Claude-Louis Navier and George Gabriel Stokes, describe the motion of fluid substances such as liquids and gases. These equations establish that changes in momentum in infinitesimal volumes of fluid are simply the sum of dissipative viscous forces (similar to friction), changes in pressure, gravity, and other forces acting inside the fluid: an application of Newton's second law.

They are one of the most useful sets of equations because they describe the physics of a large number of phenomena of academic and economic interest. They may be used to model weather, ocean currents, water flow in a pipe, flow around an airfoil (wing), and motion of stars inside a galaxy. As such, these equations in both full and simplified forms, are used in the design of aircraft and cars, the study of blood flow, the design of power stations, the analysis of the effects of pollution, etc. Coupled with Maxwell's equations they can be used to model and study magneto hydrodynamics.

The Navier-Stokes equations are differential equations which, unlike algebraic equations, do not explicitly establish a relation among the variables of interest (e.g. velocity and pressure). Rather, they establish relations among the rates of change. For example, the Navier-Stokes equations for simple case of an ideal fluid (inviscid) can state that acceleration (the rate of change of velocity) is proportional to the gradient (a type of multivariate derivative) of pressure.

Contrary to what is normally seen in solid mechanics, the Navier-Stokes equations dictate not position but rather velocity. A solution of the Navier-Stokes equations is called a velocity field or flow field, which is a description of the velocity of the fluid at a given point in space and time. Once the velocity field is solved for, other quantities of interest (such as flow rate, drag force, or the path a "particle" of fluid will take) may be found.

A two dimensional, laminar incompressible flow with constant viscosity is described by:

X-Momentum $$\rho\frac{\partial u}{\partial t}+\rho u\frac{\partial u}{\partial x}+\rho v\frac{\partial u}{\partial y}=\mu\left(\frac{\partial^2 u}{\partial x^2}+\frac{\partial^2 u}{\partial y^2}\right)-\frac{\partial \rho}{\partial x} \qquad (4.16a)$$

Y-Momentum $$\rho\frac{\partial v}{\partial t}+\rho u\frac{\partial v}{\partial x}+\rho v\frac{\partial v}{\partial y}=\mu\left(\frac{\partial^2 v}{\partial x^2}+\frac{\partial^2 v}{\partial y^2}\right)-\frac{\partial \rho}{\partial x} \qquad (4.16b)$$

And continuity $$\frac{\partial u}{\partial x}+\frac{\partial v}{\partial y}=0 \qquad (4.17)$$

Where

u = Component of Velocity in x-direction

v = Component of Velocity in y-direction

μ = Viscosity of Fluid

ρ = Density of fluid

4.3.6 Post Processing

Post- processing provides the tool with easy-to-use powerful result visualization features for structured, unstructured, and hybrid grids. It provides an in depth view of data with visualization tools such as cutting planes, contouring, streamlines, line plots, data probes and animation. Animations can be created by saving solutions with or without skipping certain number of time steps and playing the saved frames in a continuous sequence. Animations are important tools to study time-dependent developments of vertical /turbulent structures and their interaction.

CHAPTER 5

MODELLING AND ANALYSIS

5.1 IMPELLER 3D FLOW SIMULATIONS

A 3D flow simulation is carried out on an isolated impeller of a radial flow centrifugal pump on ANSYS-CFX. The procedure adopted for solving the given problem is described in the previous chapter

5.2 INITIAL DESIGN

A design code has been developed using visual C++ for calculation of design of centrifugal pump and verified with the analytical work done in the chapter 3

5.3 GEOMETRY GENERATION

Figure5.1 Front and side view of impeller

A 3D flow simulation is carried out on an isolated impeller of a radial flow centrifugal pump on ANSYS-CFX. The first task to accomplish on a numerical flow simulation is the definition of the geometry, followed by the grid generation; this step may be the most important step in this step, for the study of an isolated impeller assuming an axis symmetric flow simplifies the domain to a single blade passage.

Modelling of the impeller has been done using ANSYS–Blade modeller. The model is then meshed on Turbogrid module of ANSYS Workbench.

5.4 MESH GENERATION

Theoretically ,the errors in the solution must disappear for an increasing mesh size the selected convergence criteria are a maximum residual of 10^{-4} ,how ever it is observed that there is not much difference when mesh size is taken 20,000 and when it is 1,00,000 nodes. So 20,000 nodes are selected to reduce computational time. Figure 5.7 shows the meshing of single blade domain.

a) Maximum Face Angle

This is the greatest face angle for all faces that touch the node. For each face, the angle between the two edges of the face that touch the node is calculated. The largest angle from all faces is returned. The maximum face angle can be considered to be a measure of skewness. It should be less than 165° for improved mesh quality

b) Minimum Face Angle

This is the smallest face angle for all faces that touch the node. It is also a measure of skewness. It should be above 15° for improved mesh quality

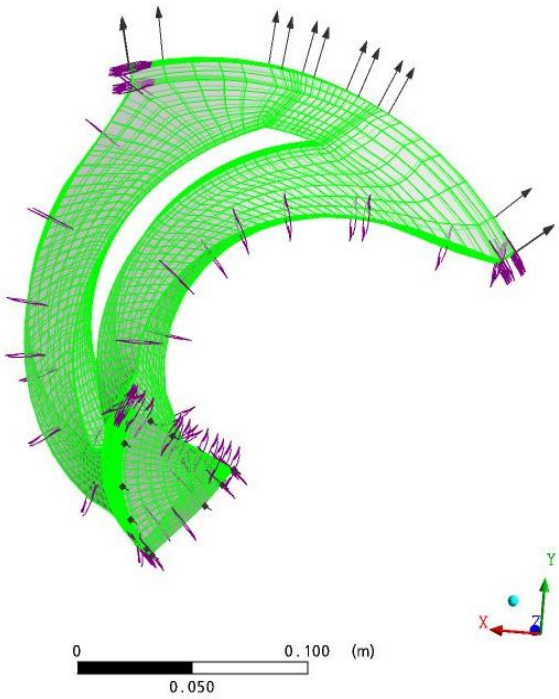

Figure 5.2 Meshing of single blade domain

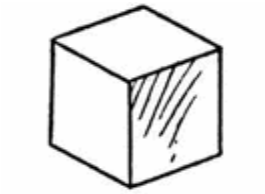

Figure 5.3 Hexahedra Brick element

Number of Nodes: 25789 (Including inlet and outlet domain)

Number of Elements: 21984 (Including inlet and outlet domain)

Type of element: Hexahedra Brick element (As shown in Figure 5.6)

Min Face angle: 25.7571 [degree]

Max Face Angle: 156.241 [degree]

5.5 PREPROCESSING

5.5.1 Simulation Parameters and Boundary Conditions

The general parameters and boundary conditions used for 3D flow simulations of the impeller are summarized in the table 5.1.

For all simulations the boundary conditions are as follows:

1) Inlet: total pressure applied in the rotation axis direction
2) Outlet: imposed mass flow
3) Periodic: two symmetry surfaces positioned in the middle of the blade passage.
4) Wall: general boundary conditions by default.

The simulation domain at the inlet and outlet sections is sufficiently extended to allow recirculation and the elliptic influence of the flow. Table 5.1 give details of impeller simulation parameters which have been defined while defining boundary conditions.

Table 5.1 Impeller Simulation parameters

Flow simulation domain	Single impeller flow channel (periodic interface)
Grid	Structured
Fluid	Water at standard conditions
Turbulence model	SST model
Discretization	Second order
Maximum residual convergence criteria	10^{-4}

5.5.2 Turbulence Model

The Shear-Stress-Transport (SST) model is developed to overcome deficiencies in the $k-\varepsilon$ and $k-\omega$ models. Therefore, using the SST model over these models is recommended. Three criteria influence the choice of turbulence model[22]

1) The physical nature of the problem

2) The quality of results required

3) Computing power

Depending on the complexity, this choice is always crucial when using CFD codes, nevertheless, the traditional turbulence models like $k-\varepsilon$ and $k-\omega$, are amply used and produce satisfactory results. It has been indicated that all turbulence models $k-\varepsilon$, $k-\omega$, SST models gave almost same identical results[20], for the same simulating conditions.

However Shear stress transport model is found to be more suitable for turbo machinery problems as they have features of both the $k-\varepsilon, k-\omega$ models. So SST model is chosen for the present work.

5.5.3 Erosion Model

Erosion is a process in which material is removed from the surface layers of an object impacted by a stream of abrasive particles. Erosion is localised in a small volume of the target material that is eventually removed. The magnitude of the wear is quantified by the volume or mass of the material that is removed by the action of the impacting particles. Experimental and computational investigations carried out by Tabakoff have contributed to understanding the mechanisms of erosion, but the detailed processes leading to material removal are still poorly understood good models for predicting the behaviour of materials during erosion are still not readily available. Finnie proposed the first analytical erosion model. These models include a variety of parameters that influence the amount of material eroded from a target surface and the mechanism of erosion. Model of Tabakoff is used for present work as its results are sufficiently good for the scope of work.

Various Coefficients for using the Tabakoff Erosion Model for Quartz – Steel[36] has been shown in the following table

Table 5.2 Coefficients for using the Tabakoff erosion model for Quartz - Steel

No.	Variable	Coefficient	Value
1	k_{12}	k_{12}	0.293328
2	Ref Velocity 1	V_1	123.72 [m/s]
3	Ref Velocity 2	V_2	352.99 [m/s]
4	Ref Velocity 3	V_3	179.29 [m/s]
5	Angle of Maximum Erosion	γ_0	30°

Sand density: 2300 kg/m^3.

Particle shape: Angular

For all cases except changing particle size common sand is taken with sizes and percentage given below in Table 5.3

Table 5.3 Sand particle size and percentage distribution

No.	Sand sizes(microns)	Percentage distribution
1	50	0.02
2	100	0.18
3	200	0.2
4	300	0.4
5	600	0.2

5.6 SOLVER

There are several methods of discretizing a given differential equation, but finite volume is used in ANSYS-CFX. The finite volume method is a numerical method for solving partial differential equations that calculates the values of the conserved variables averaged across the volume. One advantage of the finite volume method over finite difference methods is that it does not require a structured mesh (although a structured mesh can also be used). Furthermore, the finite volume method is preferable to other methods as a result of the fact that boundary conditions can be applied noninvasively. This is true because the values of the conserved variables are located within the volume element, and not at nodes or surfaces. Finite volume methods are especially powerful on coarse non uniform grids and in calculations where the mesh moves to track interfaces or shocks.

CHAPTER 6

RESULTS AND DISCUSSIONS

---

6 .1 DESIGN OF IMPELLER

The design data can be verified from the analytical work done in the chapter 3 and summarized in table 3.1

1) Specific speed of the pump is:	24.6832
2) Hydraulic efficiency of the pump:	0.6436
3) Mechanical Efficiency of the pump:	0.77688
4) Input power of the pump:	7.63732 HP
5) Input power of the pump:	5689.8 Watts
6) Torque:	37472.5 N-m
7) Diameter of the Shaft:	0.0196902 meters
8) Axial velocity:	2.54876
9) Eye diameter:	0.101375 meters
10) Inlet blade diameter:	0.0963058 meters
11) Hub diameter:	0.0236283 meters
12) Width at inlet:	0.021342 meters
13) Inlet blade velocity:	7.3115 meter per second
14) Inlet blade angle	21.9318 degree
15) Outlet blade velocity:	20.5262 meters per sec
16) Outlet diameter of blade:	0.270368 meters

17) Number of blades:	5
18) Breadth at outlet of blade	0.00767887 meters
19) NPSH required is:	1.6492
20) Outlet blade angle:	26 degree

6.2 WEAR PATTERN ON THE BLADE OF IMPELLER

Two locations are found to be the most easily worn: the root of each vane (i.e. near the leading edge) and the area on the blade to the suction side of the blade. This has been confirmed from the experimental data [17].

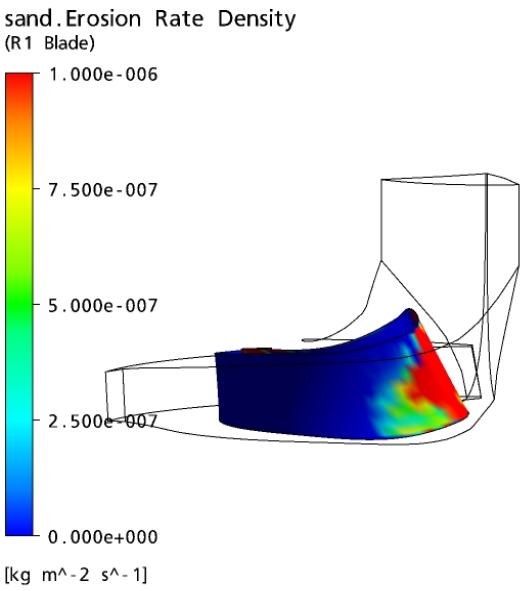

Figure 6.1: Wear on the blade on pressure side near inlet

Figure 6.1 shows the pressure side of the blade. It clearly indicates that the erosion rate is higher nearer to inlet. The sand particles strikes directly with the blades rotating at high speeds at inlet causing high wear as comparison to other parts of the impeller.

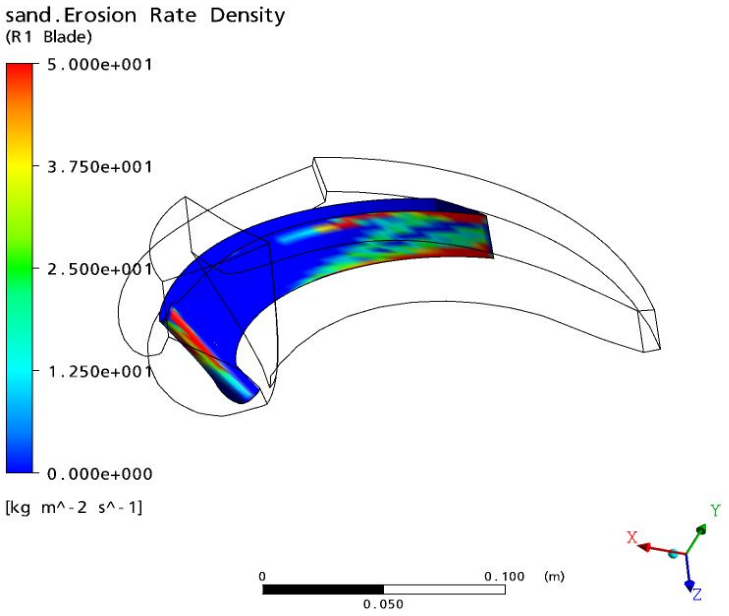

Figure 6.2 Wear of blade on suction side of blade

Figure 6.2 shows the suction side of the blade. It clearly indicates the erosion rate at inlet and at trailing edge of blade. Also erosion rate is higher nearer to the root of the blade than compared central portion of blade as shown in Figure 6.2 at the trailing edge The wear rate is higher at the roots of blade.

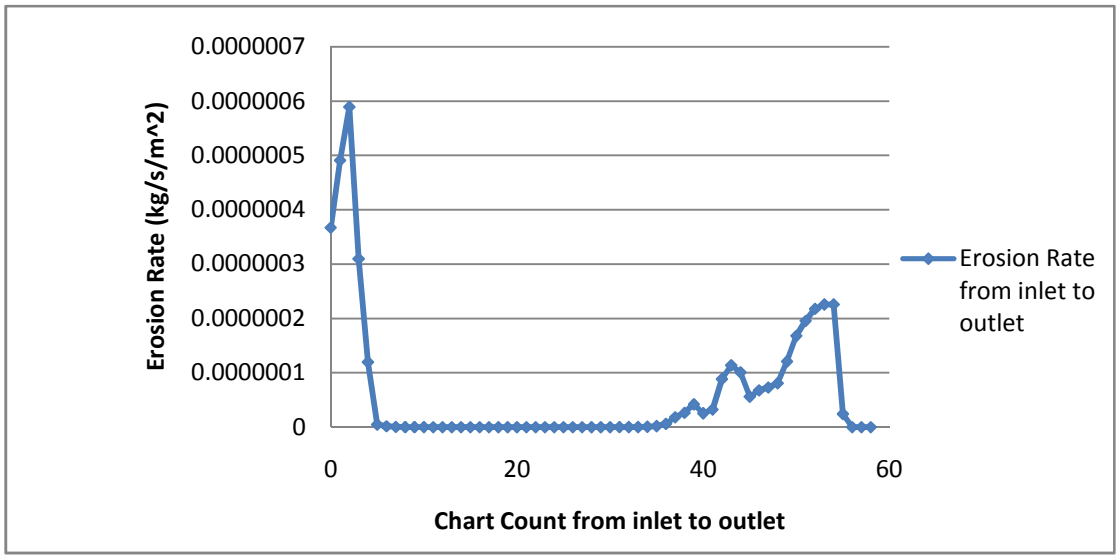

Figure 6.3 Erosion rate along streamwise direction.

Figure 6.3 shows the erosion rate along the streamwise direction from inlet to outlet. The graph shows high value of erosion rate nearer to inlet in a very limited area;

however the erosion rate at the trailing edge is less severe. The highest value of erosion rate density at inlet is three times more than erosion rate density at trailing edge .It signifies that wear pattern at inlet is more severe than wear at the trailing edge of the blade This has been visualized on Figure 6.4.

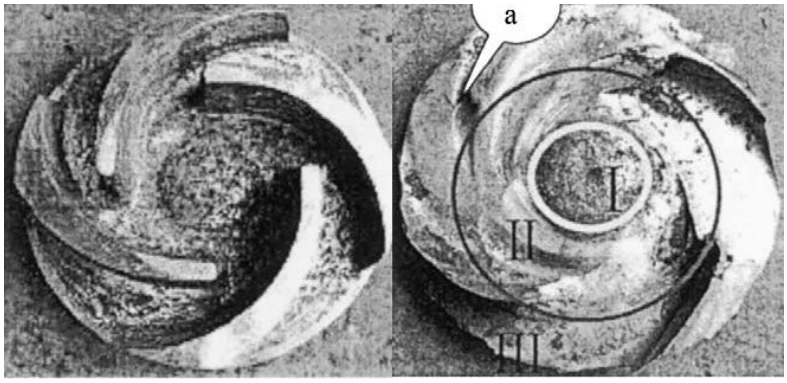

. **Figure 6.4 Experimental results shows complete wear of blades near the inlet[22]**

6.3 WEAR PATTERN ON THE HUB:

Hub is also affected by the wear. As shown in Figure 6.5 wear pattern on hub is found on the passage nearer to the inlet of the pump. As fluid moves from inlet to outlet the area of passage increases so erosion rate density decreases from inlet to outlet. Also maximum erosion of the blade is nearly 15-20 times as that of the hub.

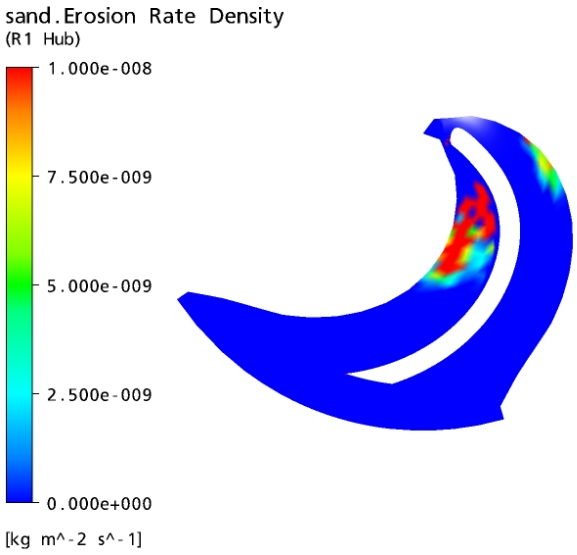

Figure 6.5 Parts of hub which are affected by the erosion

6.4 EFFECT OF PARTICLE SIZE ON EROSION RATE

The particle size of sand is varied from 100 microns to 1500 microns to see its effects on erosion of the blade. The graph shows steep increase in erosion rate density up to size of 600 microns (Figure 6.6). After 600 microns, the increase in erosion rate density is gradual.

It is also clear that the erosion rate increases as particle size increases only up to certain limit of the particle sizes. The simulation is conducted at 5%, 10% and 15 % concentration and a similar trend is observed. However, the trend in the hub is different as angle of attack is different for the blade and the hub. The graphs show increase in erosion rate up to 1000 microns only shows stability after 1100 micron particle size. As indicated in graph in Figure 6.6, there is a steep increase in erosion rate when concentration is increased. It is clearly indicative that an increase in concentration directly affects the erosion rate.

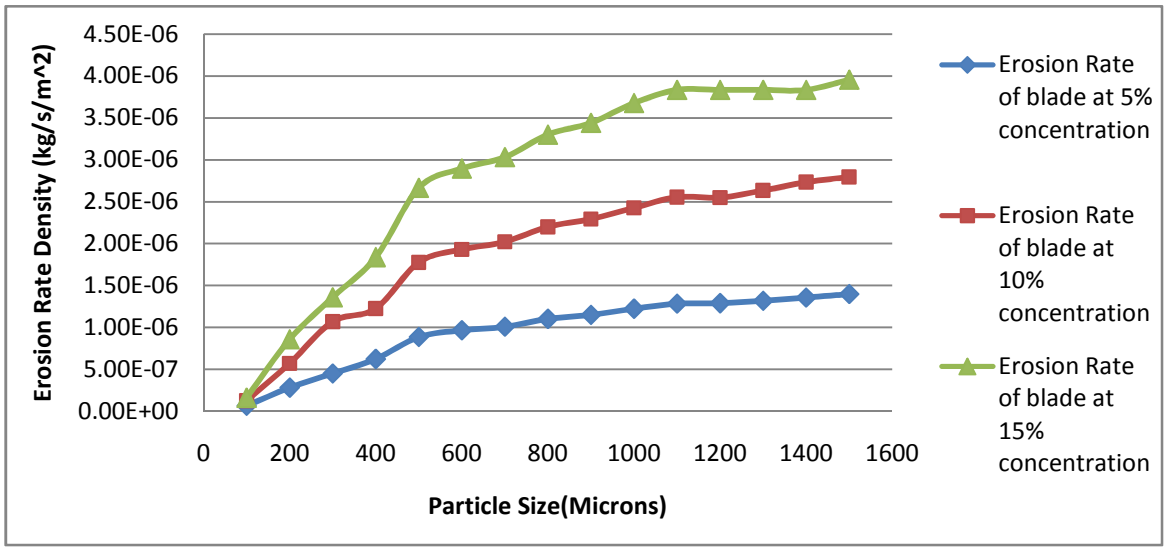

Figure 6.6 Erosion rate vs. particle size for blade at different concentrations

The erosion rate density of the blade is nearly 8-10 times greater than hub, which indicates that the hub is less prone to wear. The simulation is conducted at 5%, 10% and 15% and a similar trend is observed. The erosion rate trend of hub is totally different than that of the blade. It shows nearly equal erosion rate trend at lower values of particle size but increases to higher values above 1000 microns particle size. It clearly indicates that the manner in which erosion occurs in the blade and the hub

depends upon the manner in which particles strikes the surface. However, the graphs clearly justify the fact that blades of the impeller are more susceptible to erosion.

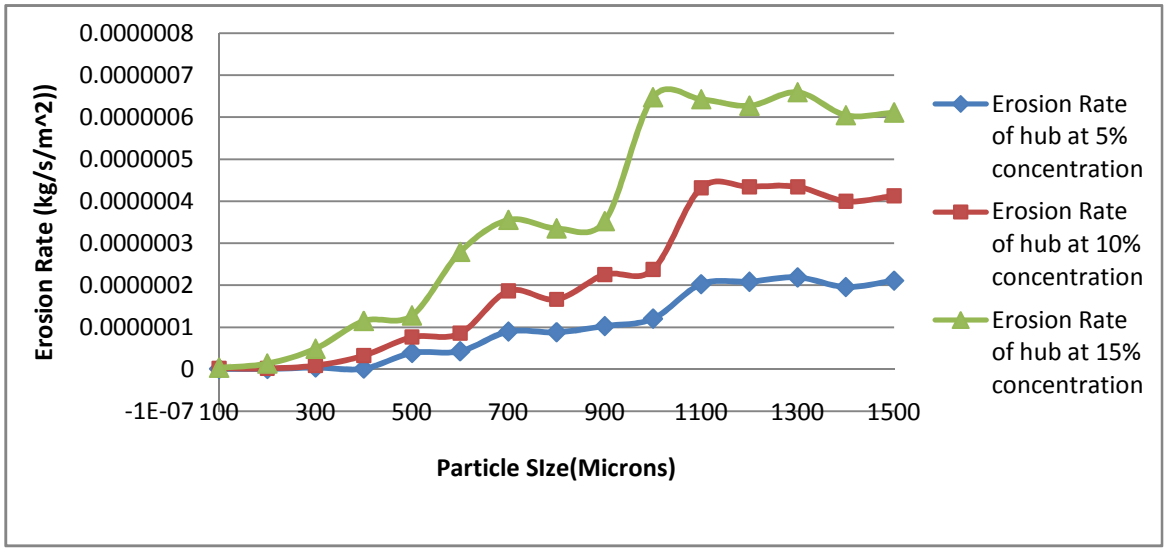

Figure 6.7 Erosion rate at varying particle size for hub

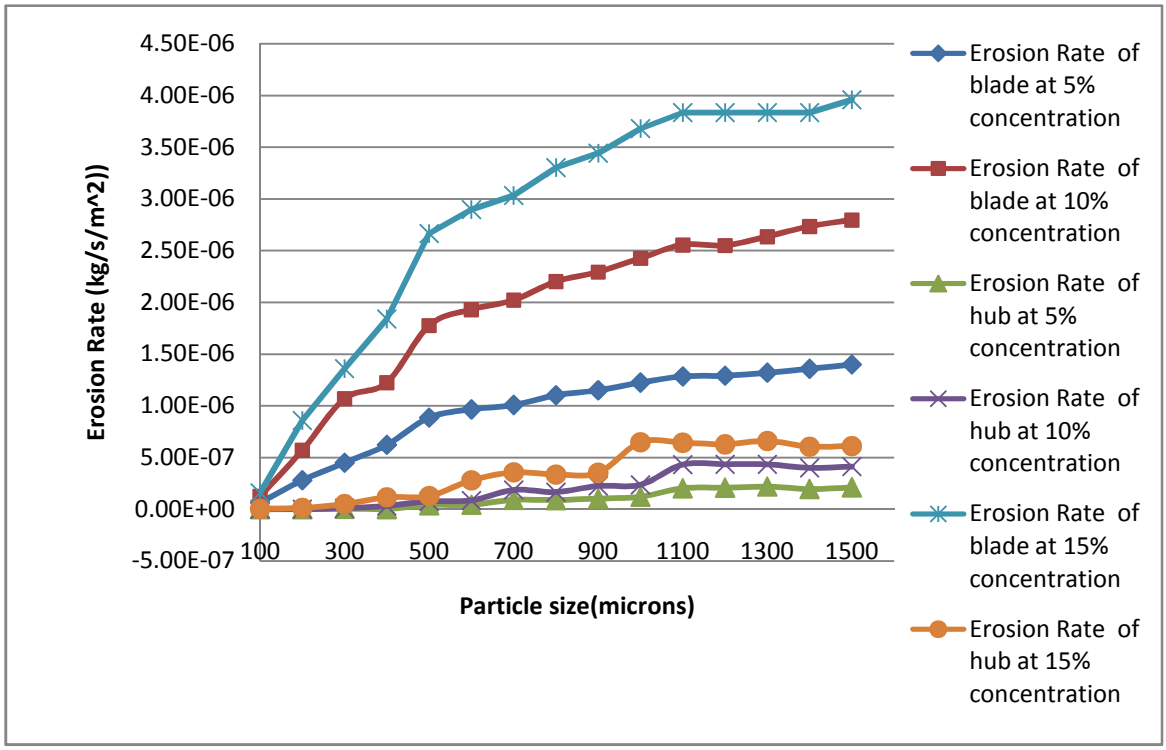

Figure 6.8 Erosion rate predictions on blade and hub at different concentrations and varying particle size

6.5 EFFECT OF FLOW RATE ON EROSION RATE

Flow rate is important parameter which causes the wear. The effect of flow rate on the erosion is most dominant. For the present case flow rate has been varied from 8 litres/s to18 litres/s.

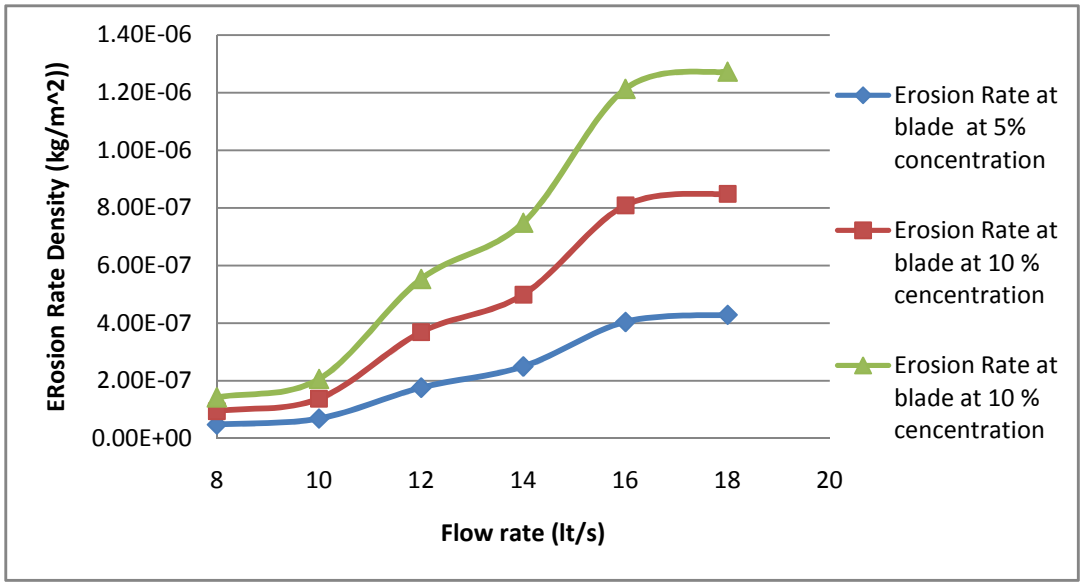

Figure 6.9 Erosion rate vs. flow rate at different concentrations on blade

The pattern of increase in erosion rate is nearly same for 5%, 10% and 15% concentration. And there is a linear increase in erosion rate with flow rate. At low flow rates the effects are negligible but as the flow rate increases, the erosion rate increases.

6. 6 EFFECT OF SPEED ON THE EROSION RATE ON BLADE AND HUB

As revolutions per minute at which impeller rotates increase, the force with which slurry strikes the impeller increases which in turn increase the erosion rate. The graphs show that the wear is more at the blades than at the hub. In case of blade there is linear increase in erosion rate with respect to increase in speed. Up to 1400 RPM there is gradual increase in erosion rate but it increases more rapidly above 1500 rpm. Similarly there is gradual increase in erosion rate density of hub at respectively lower speed, but above 1700 RPM, there is sudden increase in the erosion rate. The trends at 5%, 10% and 15% concentration are nearly same. However, there is very less effect

of concentration on erosion rate density. It justifies that the concentration has negligible effect on erosion at normal speed.

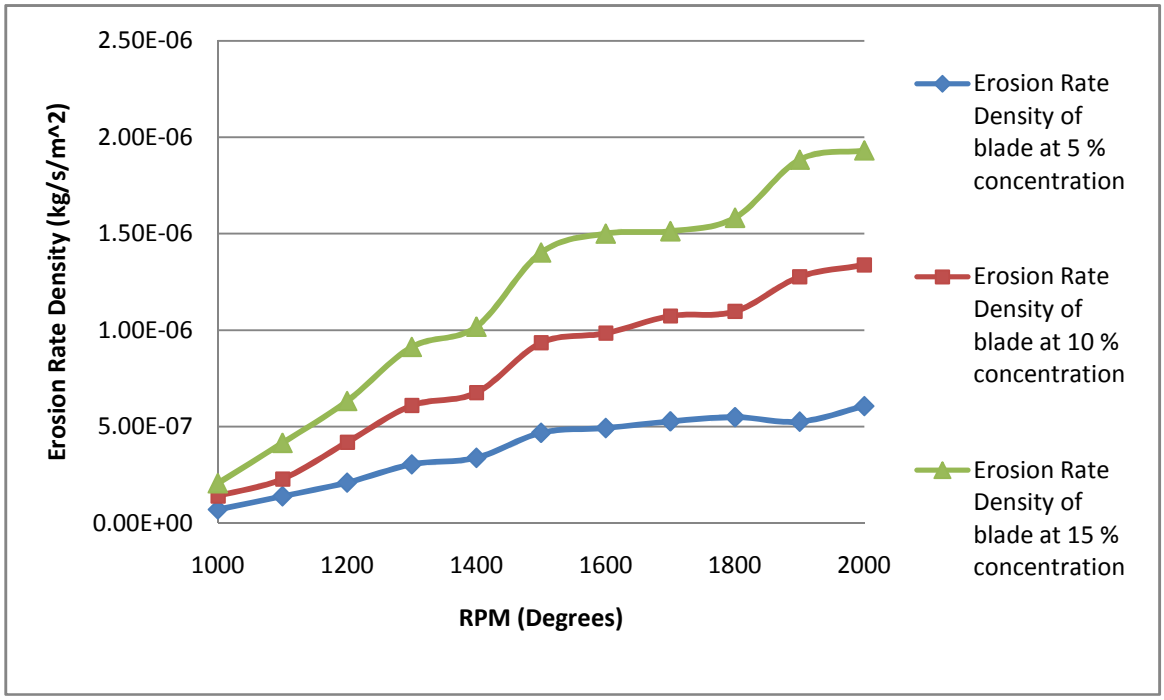

Figure 6.10 Erosion Rate vs. Speed at different concentrations on blade

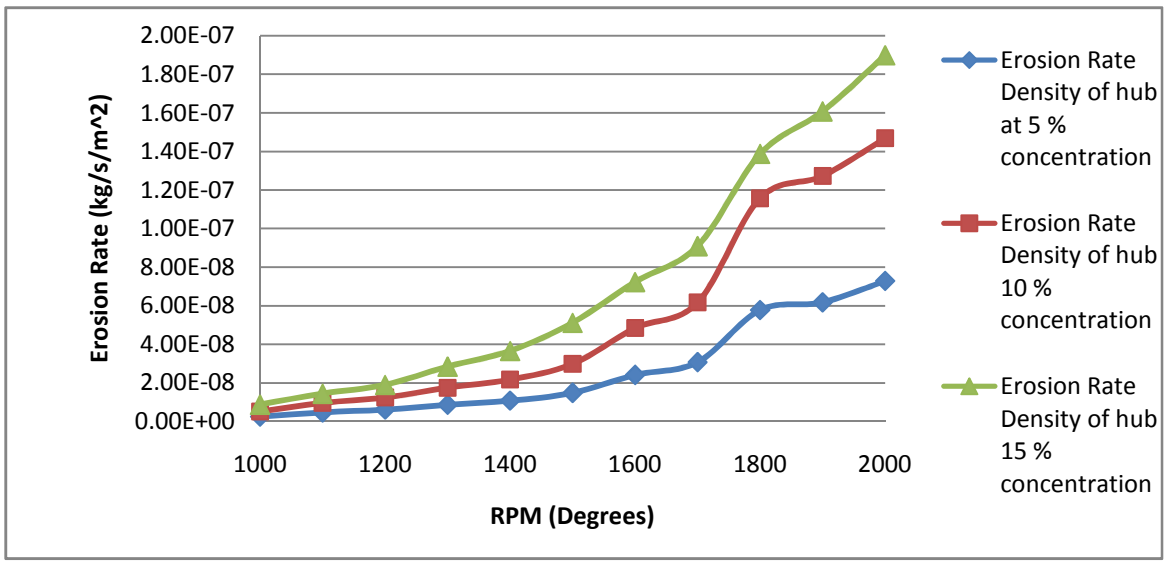

Figure 6.11 Erosion Rate vs. Speed at different concentrations on hub

The simulation has been conducted at 5%, 10% and 15% concentration and there is a huge difference between the erosion rate of hub and blade. The erosion rate density at blade is nearly 8-10 times than that of the hub.

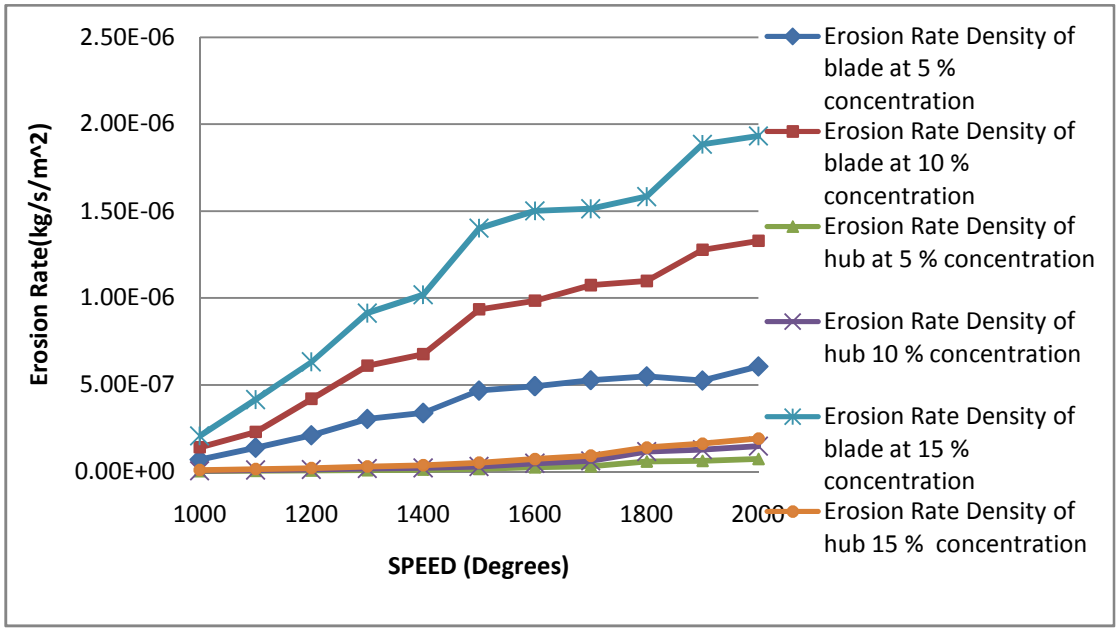

Figure 6.12 Erosion rate vs. Speed on blade and hub at different concentrations

6.7 EFFECT OF CONCENTRATION ON THE EROSION RATE ON BLADE

As the concentration of the particles in fluid increases there is negligible effect on the erosion rate on the hub, however there is linear increase in erosion rate density on the blade. Figure 6.13 shows the effect of erosion rate on the hub and the blade at varying concentration.

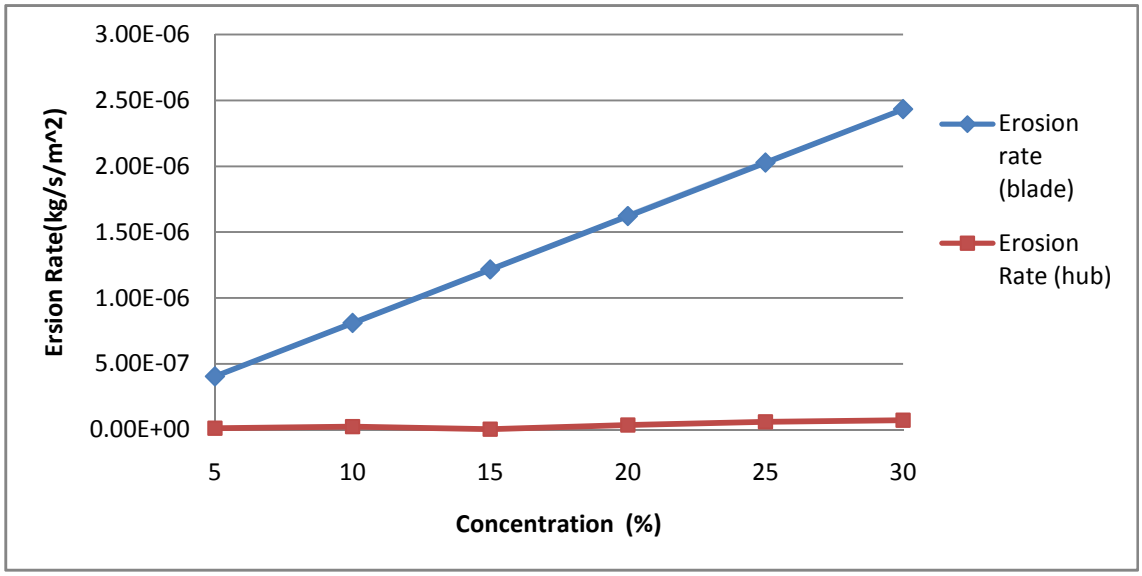

Figure 6.13 Erosion Rate vs. Concentrations at blade and hub

6.8 CALCULATION OF EROSION RATE

The erosion rate can be calculated as:

Erosion Rate (grams) =Erosion rate density*surface area*time

$$\text{Erosion rate (grams)} = \frac{\text{kg}}{\text{sm}^2} \times \text{m}^2 \times \text{s} \times 1000$$

Suppose erosion rate density for at 16 litre/s at 10% concentration is

8.08879 E -7*Area of blade*time*1000

For 100 hours of operation material eroded in grams is

8.08879E-7*0.0128465*100*3600*1000

3.740855 gm

6.9 Pressure and Velocity Distribution across Blades

The CFD simulation offers a virtual image of the internal flow in the machine allowing the analysis and the comprehension of more complex phenomena. The pressure increases from inlet of the impeller to outlet of the impeller gradually. The pressure gradually increases along streamwise direction within impeller blade-to-blade passage and has higher pressure on pressure surface than suction surface. However, the pressure developed inside the impeller is not so uniform. The isobar lines are not wholly perpendicular to the pressure side of the blade inside the impeller passage; this indicates that there could be a flow separation because of the pressure gradient effect. There is sharp drop in the pressure on the blades when flow rate is increased. This could lead to cavitation near the trailing edge of the blades. This phenomenon has been reported in the literature[9]. This can cause wear on the surface of blades on the suction side.

Figure 6.14 shows the pressure variation from inlet to outlet in a centrifugal pump impeller. Figure 6.15 and 6.16 shows pressure variation with blade to blade and meridional view respectively.

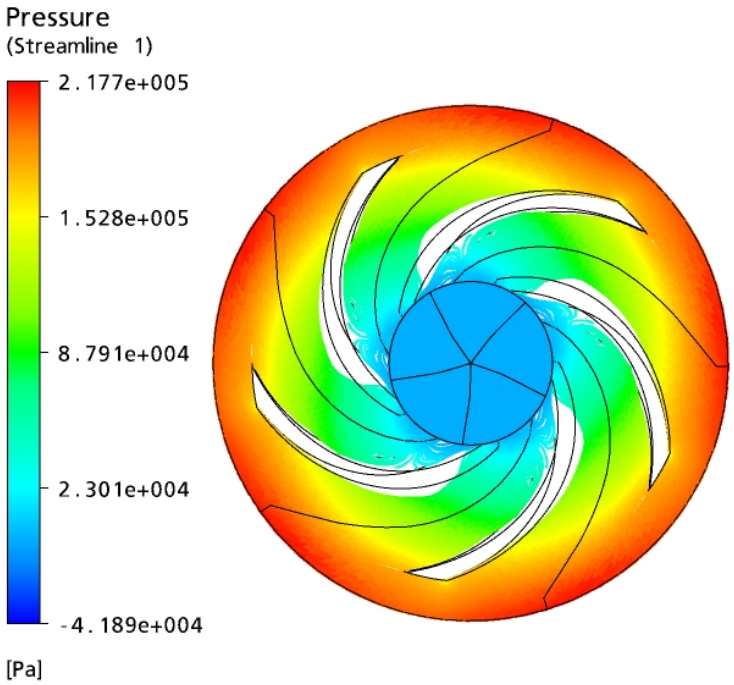

Figure 6.14 Pressure distribution from inlet to outlet

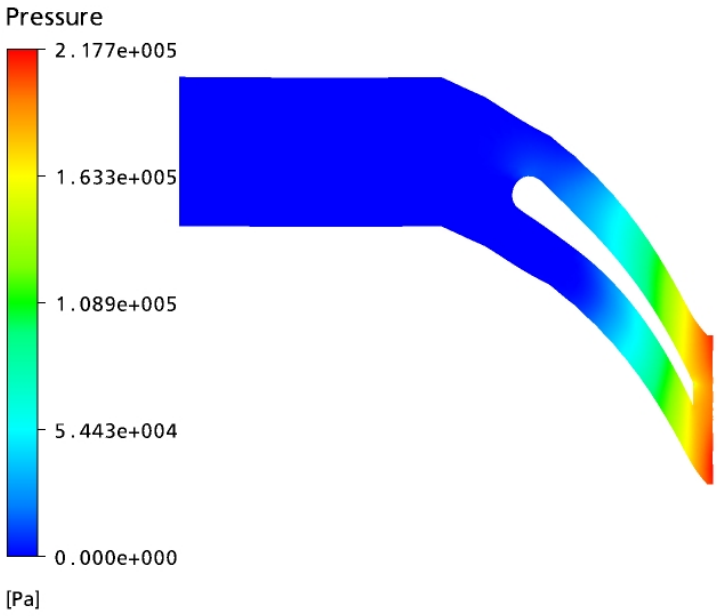

Figure 6.15 Pressure distribution (blade to blade view)

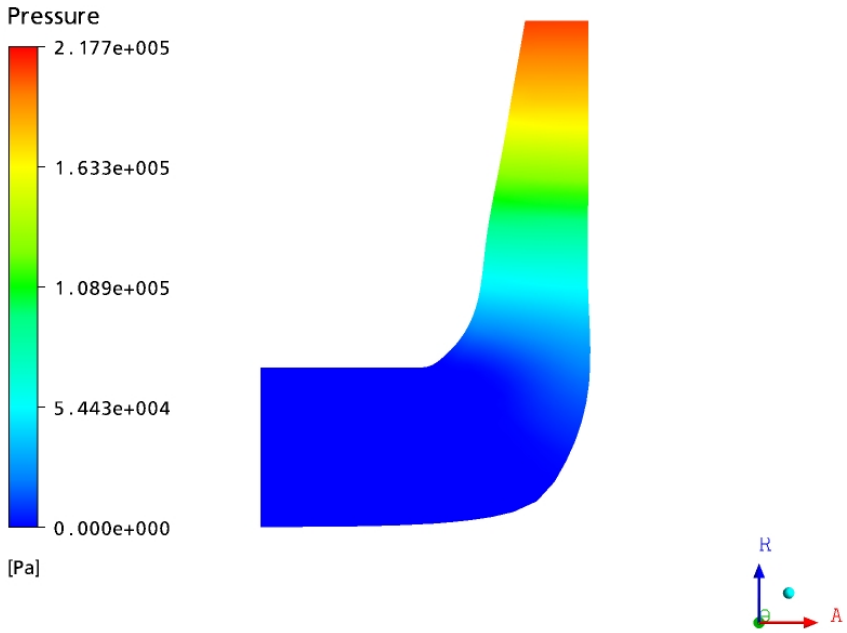

Figure 6.16 Pressure distribution (meridional view)

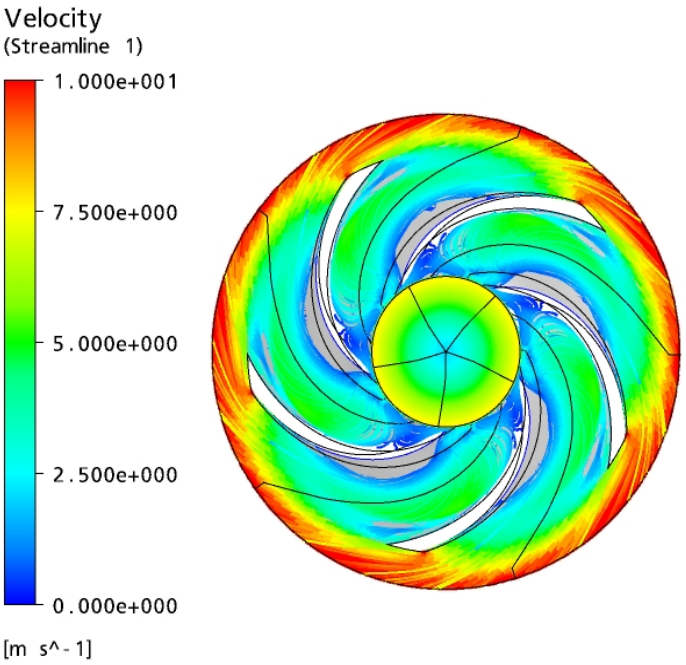

Figure 6.18 Velocity distribution from inlet to outlet

Velocity also increases gradually along streamwise direction within the impeller passage. As the flow enters the impeller eye, it gets diverted to the blade-to-blade passage. The flow at the entrance is not smooth because of the unsteady flow entering the impeller passage. The separation of flow can be seen at the blade leading edge. Since, the flow at the inlet of impeller is not tangential to the blade, the flow along the blade is not uniform and hence the separation of flow takes place along the surface of the blade. Figure 6.18 shows the velocity distribution from inlet to outlet in a centrifugal pump impeller.

CHAPTER 7

CONCLUSIONS AND SCOPE FOR FUTURE WORK

7.1 CONCLUSIONS

1) The results show that the erosion wear has strong dependence on flow rate. The higher the flow rate, the higher the wear rate of the test material. Solid concentration also affects the wear rate linearly.

2) The effect of erosion rate is more on the blades than on the hub. The graph shows that the erosion rate density on the blades is nearly 8-10 times than on the hub.

3) The effect of wear is more at leading edge than at trailing edge of blades. So selecting the optimized inlet blade angle can play a major role in reducing erosion wear and providing smooth flow for fluid.

4) The effect of particle size on the erosion rate is predominant only up to certain size limit i.e. 600-800 microns on the blades. After that, the erosion rate increases with a comparatively slower rate. This indicates that the particle size affects the erosion rate only up to certain particle size.

5) Increasing flow rate causes sharp decrease in pressure which can cause cavitation on the surface of blade.

While designing the components handling slurry, it is necessary to select proper material to increase their service life. Different methods can be used to enhance the surface properties to decrease the erosion wear and thus to increase the service life of components. Heat treatment is the best method to increase the surface hardness. Martensite structure (which has the highest hardness) can be developed on the surface of the component, thus retaining higher toughness from inside. The experiments have been conducted on the steels and it is found that the erosion rate decrease with increasing hardness by heat treatment of the steels.

Ceramic coating has been suggested[4] to protect the pump due to slurry erosion. Instead of applying coating to whole impeller, the coating can be applied only to

blade to cut manufacturing cost. Sharp corners should be avoided; the root of the blade should be round to provide smooth flow of fluid.

7.2 SCOPE OF FUTURE WORK

The use of pumps for slurry transfer has increased by several folds. The scope of future work in this topic is very vast. A lot of work can be done in this field. Better designs and improved materials can increase the life of pumps to several more hundred hours.

1) The other affecting design parameters such as inlet blade angle, outlet blade angle, and the number of blades can be changed to see the effect of erosion rate and a optimized design could be developed which will have minimum erosion on the impeller.

2) Pump performance characteristics as well as velocity and pressure distribution can be studied.

3) Different types of materials can be tested for manufacturing of impeller and erosion patterns can be studied.

4) The present work of homogeneous flow can be extended to heterogeneous flows so that the effect of erosion behaviour can be evaluated for heterogeneous slurries.

5) Effect of cavitation on pump performance and erosion wear can be studied.

REFERENCES

1. Desai P. V ,Pagalthivarthi V, Addie G. R. (1990), "Particular motion and concentration fields in centrifugal slurry pumps", Particulate Science and Technology, Vol. 8:1, pp 77 – 96

2. Achim Daniela,Alan K Easton,Phillip M. Schwarz,Peter J Witt and Zakhari (1999)**,** "Computational and experimental studies of tube erosion in a fluidised bed" , Second International Conference On CFD in the Minerals and Process Industries,CSIRO,6-8 December, pp 243-248

3..Manickam M., M.P. and Schwarz, Mcintosh M.J,(1999), "CFD analysis of erosion of bifurcation duct wall" ,Second International Conference On CFD in the Minerals and Process Industries,CSIRO,6-8 December, pp 243-248

4. Zhao H.K, Yabuki A,Matsumura M ,Takahashi,T and Yamamoto M,(1999), "Slurry erosion properties of ceramic coating", Wear,Vol. 233-235, pp 608-614.

5. Anders Sellgren, Addie Graeme and Yu Wi-Chung, (1999), "Effects of non-newtonian mineral suspensions on the performance of centrifugal pumps", Mineral Processing and Extractive Metallurgy Review, Vol20:1, pp 239 – 249

6. Lee S. Y., Dimenna R. A., and Duignan M. R. 2001, "Designing a scaled erosion test with CFD methods", U.S. Department of Energy WSRC-MS-2001-00500

7. Gandhi B.K, Singh S. N., Seshadri V. 2001, "Performance characteristics of centrifugal slurry pumps", Journal of Fluids Engineering ,Vol. 123, pp 271-280

8. Hawthorne H.M. 2002, "Some Coriolis slurry erosion test developments", Tribology International, Vol. 35 ,pp 625–630

9. Bakir F., Kouidri S., Belamri T., and Rey R.,(2001), "On a general method of unsteady potential calculation applied to the compression stages of a turbo machine—Part I: Theoretical approach," Journal of Fluids Engineering, Vol. 123, no. 4, pp. 780–786.

10. Clark H. McI. , (2002), "Particle velocity and size effects in laboratory slurry erosion measurements or do you know what your particles are doing", Tribology International, Vol. 35, pp 617–624

11. Zhou Weidong, Zhao Zhimei, Lee T. S. and Winoto S. H,(2003), "Investigation of flow through centrifugal pump impellers using computational fluid dynamics", International Journal of Rotating Machinery, Vol. 9,Issue 1, pp 49-61

12.. Hamed Awatef A., Tabakoff Widen, Rivir Richard B., Das Kaushik, Arora Puneet,(2002), "Turbine blade surface deterioration by erosion", Journal of Turbomachinery, July Vol 127, Issue 3, pp. 445-452

13. Engin T, Gur M, 2003, "comparative evaluation of some existing correlations to predict head degradation of centrifugal slurry pumps", Journal of Fluids Engineering, Vol. 125, pp 149-157

14. Clark H.McI. 2004, "The influence of the squeeze film in slurry erosion", Journal of Wear, Vol. 256 , pp 918–926

15. Gandhi B K., Borse Satish V. 2004, "Nominal particle size of multi-sized particulate slurries for evaluation of erosion wear and effect of fine particles", Journal of Wear, Vol. 257 , pp 73-79

16. Rajesh J. John, Bijwe J., Venkataraman B., Tewari U.S. 2004, "Effect of impinging velocity on the erosive wear behaviour of polyamides", Tribology International Vol. 37 , pp 219-226

17. Wang Yao, Zuo Ming J., and Fan Xianfeng 2005, "Design of an experimental system for wear asssessment of slurry pumps", Proceeding of the 2nd CDEN-conference 2005, Kananaskis, University of Calgary

18 Tian Harry H., Graeme R. Addie 2005, "Experimental study on erosive wear of some metallic materials using Coriolis wear testing approach", Journal of Wear vol. 258 , pp 458–469

19. Asuaje Miguel, Bakir Farid, Kouidri Smaine, Kenyery Frank, Rey Robert 2005, "Numerical modelization of the flow in centrifugal pump: Volute Influence in

Velocity and Pressure Fields", International Journal of Rotating Machinery Vol.(2005:3), pp 244–255

20. Tian Harry H., Addie Graeme R.,Pagalthivarthi Krishnan V. 2005, "Determination of wear coefficients for erosive wear prediction through Coriolis wear testing", Journal of Wear, Vol. 259 ,pp 160–170

21. Das S.K, Godiwalia K.M, Mehrotra S P, Sastry K K M and Dey P K 2006, "Analytical model for erosion behaviour of impacted fly-ash particles on coal-fired boiler components" , Sadhana, Vol. 31, Part 5, pp. 583–595

22. Li Ping, Cai Qizhou, Wei Bokang 2006, "Failure analysis of the impeller of slurry pump used in zinc hydrometallurgy process", Engineering Failure Analysis Vol. 13, pp 876–885.

23. Roudnev A, Kosmicki R 2007, "Effects of CFD modelling configuration on centrifugal slurry pump casing wear prediction", The 17th International Conference on the Hydraulic Transport of Solids

24. Shah Subhash N, Jain Samyak,(2007), "Coiled tubing erosion during hydraulic fracturing slurry flow", Journal of Wear, Vol. 264 , pp 279–290

25. Desale Girish R., Gandhi B.K., Jain S.C.,(2007), "Slurry erosion of ductile materials under normal impact condition", Journal of Wear, Vol. 264, pp 322–330

26. Kergourlay G.,M., Bakir Younsi F., and Rey R.(2007), "International journal of rotating machinery", Vol 2007, Article ID 85024,13 pages

27. Cheah K.W, Lee T. S. ,Winoto S. H., and Zhao Z.M. ,(2007), "Numerical flow simulation in a centrifugal pump at design and off-design conditions", International Journal of Rotating Machinery,Vol (2007), Article ID 83641, 8 page

28. Feng Jianjun, Karl Friedrich, and Dohmen Hans Josef, (2007), "Numerical investigation on pressure fluctuations for different configurations of vaned diffuser pumps", International Journal of Rotating Machinery ,Vol 2007, Article ID 34752, 10 pages

BIBLIOGRAPHY

29. A.J Stepanoff,(1958), "Centrifugal and axial flow pumps theory design and application", 2nd ed, John wilay and sons, New York

30. A .J Stepanoff,(1965), **"**Pumps and blowers and two-phase flow", John wilay and sons, New York

31. John Evans Miller, Frederick Schmid,(1987), "Slurry erosion: uses, applications, and test methods: a Symposium", Astm International

32. Labanoff Val S,(1992), "Centrifugal pumps design and applications", 2nd edition Gulf Publishing Company.

33. Vasandani V.P., (1993), "Hydraulic machines theory and design", 10th edition, Khanna Publishing house, New Delhi.

34. P.S Ghoshdastidar (1998), "Computer simulation of flow and heat transfer", 1998, Tata McGraw-Hill.

35. John Tuzson, (2000),"Centrifugal pump design", September 2000, Wiley publisher

36. Igor J Karassik,(2001), "Pump handbook", Third Edition, McGraw-Hill Professional

37 Robert Lafore, (2005), "Object oriented programming in turbo C++", Galgotia publications pvt ltd

38. ANSYS CFX-Manual,(2006),Published by, ANSYS CFX, Release 11.0, December, 2006, ANSYS, Inc.

ANNEXURE I

PROGRAM FOR DESIGN OF CENTRIFUGAL PUMP

```
#include<stdafx.h>

#include<iostream>

using namespace std;

double a,b,c,u1;

void fn_Roots()

{

	double D = (b*b-4*a*c);
	if(D>=0)
	{
		double x1 = (-b+sqrt(D))/(2*a);
		double x2 = (-b-sqrt(D))/(2*a);
		if(x1>=0)
		{
			u1=x1;
		}
		if(x2>=0)
		{
			u1=x2;
		}
	}
	if(D<0)
		cout<<"\nEquation has imaginary roots"<<endl;

}
```

```
void main()
{
        //Enter the input parameters//
        double H,Q,p,N,Ns,Pin,P;
        double  Oeff,Pw,Heff,Meff,Veff,pi=3.1415;
        double theta=3.143*22/180,g=9.81,C1m,beta1;
        double
        Q1,De,Ca,B1,b1,b2,a1,a2,a3,Beta2,C2,C3,u2,D1,Dh,Hr,C2m,w,dH,beta;
        double T,Dsh,D2,D,b0,Ts,Cl,G1;
        double phi,sai,Hs,w1,s1,r1;
        double R,R1,dr=0.002;
        int       z;
        const double    r=1000;          //Density of water
        const double    s=25;   //Shear stress of the shaft
        const double    sigma=1.1;      //Varies from 0.9-1.1
        const double    tow=1.05;       //Varies from 1.05-1.1
        const double    k=0.84;          //Varies from 0.75-0.85
        const double    beta3=17.5*3.1415/180;
        //h=Head
        //q=Flow Rate
        //p=N*sqrt(Q) term used in calculation of specific speed
        //Ns=Specifc speed
```

```
cout<<"**********************************************************
**********"<<endl;

cout<<"PROGRAM FOR THE INPUT PARAMETERS FOR THE DESIGN
OF CENTRIFUGAL PUMP IMPELLER"<<endl;

cout<<"**********************************************************
**********";

cout<<"\nEnter the value of desired head of the pump (meters):  "<<"\t";

cin>>H;

cout<<"\nEnter the value of desired flow rate (m^3 per sec):  "<<"\t";

cin>>Q;

cout<<"\nEnter the value of desired speed of the pump (rpm):  "<<"\t";

cin>>N;

cout<<"\nEnter the value of overall efficiency of pump (%):  "<<"\t";
//Take the value from the Stepanoff's curves

cin>>Oeff;
cout<<"\nEnter the value of Vol. efficiency of the pump(%):  "<<"\t";
//Normally varies from 0.85 to 0.98

cin>>Veff;
cout<<"**********************************************************
**********";

cout<<"\nCONSTANTS USED IN THE CALCULATION \n"       ;

cout<<"**********************************************************
***  **********";

cout<<"\n\nDensity of water(r):"<<"\t\t\t\t"<<r<<" kg/cubic metre";

cout<<"\nAccleration due to gravity(g):"<<"\t\t\t"<<g<<" metre per sec sqr";

cout<<"\nShear stress of the shaft in MPa(s):"<<"\t\t\t"<<s;
```

```
cout<<"\nsigma:"<<"\t\t\t\t\t\t"<<sigma;

cout<<"\ntow:"<<"\t\t\t\t\t\t"<<tow;

cout<<"\nk:"<<"\t\t\t\t\t\t"<<k;

cout<<"\n**************************************************
**********";

cout<<"\nRESULTS OF THE GIVEN INPUT"<<"\n";

cout<<"\n**************************************************
**********";

p=N*sqrt(Q);

Ns=p/pow(H,0.75);                    //Calculation of specific speed

cout<<"\nSpecfic speed of the pump is"<<": "<<"\t\t\t"<< Ns <<"\n\n";

//The values of Ns and Q are used to get the value for overall efficiency from
the  Stepanoffs curve

Heff=1-(0.66*(1-Oeff));              //Using Wislicenus formula for finding
hydraulic efficiency

cout<<"\nHydrualic efficiency of the pump :"<<"\t\t\t"<<Heff<<"%"<<"\n\n";

Meff=(Oeff)/(Heff*Veff);

cout<<"\nMechanical Eff. of the pump: "<<"\t\t\t"<<Meff<<"%"<<"\n\n";

P=(r*g*Q*H)/(745*Oeff);

Pin=1.15*P;                          //Keeping the margin of 15%

Pw=Pin*745;

cout<<"\nInput power of the pump:   "<<"\t\t\t"<<Pin<<" HP "<<endl;

cout<<"\nInput power of the pump: "<<"\t\t\t"<<Pw<<" Watts "<<endl;

//Calculation of Shaft diameter
```

```
T=Pw*60*1000/(2*pi*N);
cout<<"\nTorque: "<<"\t\t\t\t\t\t"<<T<<endl;
D=16*T/(pi*s);
Dsh=pow(D,0.333333);
cout<<"\nDiameter of the Shaft:  "<<"\t\t\t\t"<<Dsh<<" mm"<<endl;
        Q1=Q+(Q*0.08);
        a1=sigma*sigma*tan(beta3)*tan(beta3);
        a2=tow*tow*k;
        a3=a1/a2;
        a=pow (a3,0.3333);
        b1=N*N*Q1;
        b=pow (b1,0.3333);
        Ca=0.152*a*b;                   //Axial velocity
        cout<<"\nAxial velocity: "<<"\t\t\t\t\t"<<Ca<<endl;
        De=sqrt((4*Q1)/(pi*k*Ca));              //Dia of eye
        cout<<"\nEye diameter: "<<"\t\t\t\t\t\t"<<De<<" meters"<<endl;
        D2=0.95*De;
        cout<<"\nInlet blade diameter: "<<"\t\t\t\t\t"<<D2<<" meters"<<endl;
        C3=Ca*1.05;
        C2=1.1*C3;
        Dh=1.2*Dsh;
        cout<<"\nHub diameter: "<<"\t\t\t\t\t\t"<<Dh<<" mm"<<endl;
        b2=(Q1)/(pi*D2*C3);
```

```
cout<<"\nWidth at inlet: "<<"\t\t\t\t\t"<<b2<<" meters"<<endl;

u2=(pi*D2*N)/(60);

cout<<"\nInlet blade velocity: "<<"\t\t\t\t\t"<<u2<<" meter per
second"<<endl;

//Inlet blade velocity

beta=atan(C2/u2);

Beta2= beta * 180/3.1415;

cout<<"\nInlet blade angle"<<"\t\t\t\t\t"<<Beta2<<" degree"<<endl;
//Inlet blade angle

double pq=0.32;
//Varies from 0.28 to 0.32

double ang=26*3.1415/180;

double outang=ang*180/3.1415;
// Value recomended by Stepnoff's

Hr=((1+pq)*H)/Heff;

C2m=1.1*C3;
// meridional flow velocity

C1m=0.9*C2m;

a=1;

b=-(C2m)/(tan(ang));

c=-(Hr*9.81);

fn_Roots();
//Call of function for calculation of roots of quadratic equation

cout<<"\nOutlet blade velocity: "<<"\t\t\t\t\t"<<u1<<" meters per
sec"<<endl;
```

```
D1 = (60*u1)/(pi * N);
//CALCULATION OF NUMBER OF BLADES

cout<<"\nOutlet diameter of blade: "<<"\t\t\t\t"<<D1<<"
meters"<<endl;

z=2*pi*sin(theta)*((D2+D1)/(D1-D2));

cout<<"\nNumber of blades: "<<"\t\t\t\t\t"<<z+1<<endl;

B1=(Q1)/(pi*D1*C1m);

cout<<"\nBreadth at outlet of blade"<<"\t\t\t\t"<<B1<<"
meters"<<endl;

double t1=0.3,t2=1.2;                                    //
CALCULATION OF NPSH

w=C3/sin(beta3);

dH=((t1*w*w)+(t2*C3*C3))/(2*g);

cout<<"\nNPSH Required is:"<<"\t\t\t\t\t"<<dH<<endl;

cout<<"\nOutlet blade angle: "<<"\t\t\t\t\t"<<outang<<"
degree"<<"\n\n";

cout<<"**************************************************
**************************";


}
```

ANNEXURE II

OUTPUT OF THE PROGRAM

****

PROGRAM FOR THE INPUT PARAMETERS FOR THE DESIGN OF CENTRIFUGAL PUMP IMPELLER

****

ENTER THE VALUE OF DESIRED HEAD OF THE PUMP (METERS): 14.5

ENTER THE VALUE OF DESIRED FLOW RATE (M^3 PER SEC): 0.016

ENTER THE VALUE OF DESIRED SPEED OF THE PUMP (RPM): 1450

ENTER THE VALUE OF OVERALL EFFICIENCY OF PUMP (%): 0.46

ENTER THE VALUE OF VOL. EFFICIENCY OF THE PUMP (%): 0.92

****

CONSTANTS USED IN THE CALCULATION

****

DENSITY OF WATER(R): 1000 KG/CUBIC METRE

ACCLERATION DUE TO GRAVITY (G): 9.81 METRE PER SEC SQR

SHEAR STRESS OF THE SHAFT IN MPA(S): 25

SIGMA: 1.1

TOW: 1.05

K: 0.84

****

RESULTS OF THE GIVEN INPUT

****

SPECFIC SPEED OF THE PUMP IS:	24.6832
HYDRUALIC EFFICIENCY OF THE PUMP:	0.6436%
MECHANICAL EFFICIENCY OF THE PUMP:	0.77688%
INPUT POWER OF THE PUMP:	7.63732 HP
INPUT POWER OF THE PUMP:	5689.8 WATTS
TORQUE:	37472.5
DIAMETER OF THE SHAFT:	19.6902 MM
AXIAL VELOCITY:	2.54876
EYE DIAMETER:	0.101375 METERS
INLET BLADE DIAMETER:	0.0963058 METERS
HUB DIAMETER:	23.6283 MM
WIDTH AT INLET:	0.021342 METERS
INLET BLADE VELOCITY:	7.3115 METER PER SECOND
INLET BLADE ANGLE	21.9318 DEGREE
OUTLET BLADE VELOCITY:	20.5262 METERS PER SEC
OUTLET DIAMETER OF BLADE:	0.270368 METERS
NUMBER OF BLADES:	5
BREADTH AT OUTLET OF BLADE	0.00767887 METERS
NPSH REQUIRED IS:	1.6492
OUTLET BLADE ANGLE	26 DEGREE

****